Published in final edited form as:

Nature. 2019 October ; 574(7778): 359–364. doi:10.1038/s41586-019-1647-8.

Regulation of Lifespan by Neural Excitation and REST

Joseph M. Zullo[1,*], **Derek Drake**[1,*], **Liviu Aron**[1], **Patrick O'Hern**[1], **Sameer C. Dhamne**[2], **Noah Davidsohn**[1], **Chai-An Mao**[3], **William H. Klein**[4], **Alexander Rotenberg**[2], **David A. Bennett**[5], **George M. Church**[1], **Monica P. Colaiácovo**[1], **Bruce A. Yankner**[1]

[1]Department of Genetics, Harvard Medical School, Boston, MA 02115

[2]F.M. Kirby Neurobiology Center, Department of Neurology, Boston Children's Hospital, Harvard Medical School, Boston, MA 02115

[3]Department of Ophthalmology and Visual Science, The University of Texas McGovern Medical School, Houston, TX 77030

[4]Department of Systems Biology, The University of Texas MD Anderson Cancer Center, Houston, TX 77030

[5]Rush Alzheimer's Disease Center, Rush University Medical Center, Chicago, IL 60612

Abstract

The mechanisms that extend lifespan in humans are poorly understood. Here we show that extended longevity in humans is associated with a distinct transcriptome signature in the cerebral cortex characterized by downregulation of genes related to neural excitation and synaptic function. In the model system *C. elegans*, neural excitation increases with age and inhibition of excitation globally, or in glutamatergic or cholinergic neurons, increases longevity. Furthermore, longevity is dynamically regulated by the excitatory-inhibitory balance of neural circuits. The REST transcription factor is upregulated in humans with extended longevity and represses excitation-related genes. Notably, REST-deficient mice exhibit increased cortical activity and neuronal excitability during aging. Similarly, loss-of-function mutations in the *C. elegans* REST orthologs

Correspondence should be addressed to: Bruce A. Yankner, Department of Genetics, Harvard Medical School, 77 Avenue Louis Pasteur, NRB-858C, Boston, MA 02115, Ph: 617-432-6800; Fax: 617-432-6825, bruce_yankner@hms.harvard.edu. **Corresponding author:** Correspondence and requests for materials should be addressed to B.A.Y. (Bruce_Yankner@hms.harvard.edu).

*These authors contributed equally to this work.

Author Contributions: J.Z., P.O., and N.D. performed experiments in *C. elegans*, D.D. performed statistical analysis and informatics on human brain and *C. elegans* RNA-seq, L.A. and D.D. analyzed REST cKO mice and human brain sections, L.A. S.D., and A.R. performed PET-CT and electrophysiological analysis of mice, J.Z. performed cell culture, C.-A.M., W.K. and G.M.C. contributed reagents, and D.B. contributed brain samples and data from the ROSMAP cohort. J.Z., D.D., M.C. and B.A.Y. contributed to the overall study design. B.A.Y. directed the study and B.A.Y., J.Z., and D.D. wrote the manuscript, which was examined by all authors.

Supplementary Information is available in the online version of the paper.

Ethics Declarations:

GMC is a cofounder and senior advisor for GC Therapeutics, Inc., which uses transcription factors for therapeutics.

Data Availability: Data from the ROSMAP cohort are available under controlled use conditions set by human privacy regulations. To access the data, a data use agreement is needed. This registration is in place solely to ensure anonymity of the ROSMAP study participants. Data can be requested on the Rush Alzheimer's Disease Center Resource Sharing Hub at www.radc.rush.edu. *C. elegans* RNA-seq data are available in the Gene Expression Omnibus (GEO) under accession number GSE123146.

Code Availability: All code used in the analysis of data presented in this manuscript is available upon request.

spr-3 and *spr-4* elevate neural excitation and reduce the lifespan of long-lived *daf-2* mutants. In wild-type worms, *spr-4* overexpression suppresses excitation and extends lifespan. REST, SPR-3/4 and reduced excitation activate the longevity-associated transcription factors FOXO1 and DAF-16 in mammals and worms, respectively. These findings reveal a conserved mechanism of aging mediated by neural circuit activity and regulated by REST.

Studies in invertebrate and mammalian models suggest that the nervous system plays a role in the regulation of aging[1, 2]. In the nematode *C. elegans*, ablation of specific sensory or neurosecretory neurons alters lifespan [3–6], and lifespan extension from reduced insulin/IGF-like signaling can be reversed by restoring function specifically in neurons[7]. However, whether the activity state of the nervous system impacts the aging process is unresolved. Here, we describe a conserved mechanism of aging mediated by global neural activity and regulated by REST.

Neural excitation and longevity

Previous studies of the aging human brain have shown dynamic gene expression changes that distinguish young adults from the aging population[8]. However, the recent expansion of human aging cohorts has increased the statistical power for partitioning the aging population into subgroups based on transcriptome profiling. To gain insight into gene expression changes in the brain associated with extended human longevity, we analyzed RNA-seq[9, 10] and microarray data[11] from the frontal cortex of aged individuals with intact cognitive function in three different cohorts. Age-associated genes were compared between all individuals and Pearson correlation coefficients were derived. Hierarchical clustering suggested that the aging population partitioned into three groups (Extended Data Fig. 1a–c). The most significant changes associated with the extended longevity groups (≥85 versus ≤80 years of age) were downregulation of neural excitation/synaptic function genes and upregulation of immune function genes (Fig. 1a–d, Extended Data Fig. 1d–f, Supplementary Tables 1–6). This did not change after adjusting for the presence of amyloid deposits and neurofibrillary tangles in the ROSMAP cohort (data not shown). Meta-analysis of gene ontology (GO) enrichment in each cohort indicated that terms related to excitatory, but not inhibitory synaptic transmission were enriched in the downregulated genes (Extended Data Fig. 1g, Supplementary Table 7). These results suggest that extended human longevity may be associated with reduced excitatory neurotransmission.

To explore the neural regulation of longevity, we utilized *C. elegans*, a well-established model system of aging. Neural excitation in *C. elegans* was monitored by GCaMP calcium imaging in the glutamatergic ASH neurons[12]. In wild-type worms, rapid, transient pulses of GCaMP fluorescence indicative of neuronal excitation were observed (Supplementary Video 1). Calcium influx in ASH neurons increased significantly during normal aging from adult day 1-2 to day 12-16 (Fig. 1e). To determine the effect of decreasing calcium influx on lifespan, worms were treated with nemadipine, an inhibitor of L-type calcium channels that reduces neural excitation (Fig. 1f). Continuous treatment with nemadipine beginning at adult day 1 significantly extended lifespan (Fig. 1g). Moreover, incubation of worms with ivermectin, an agonist of invertebrate glutamate-gated chloride channels, suppressed neural

excitation and resulted in a dose-dependent extension of mean lifespan (Fig. 1h, i). Nemadipine and ivermectin also extended lifespan when administered at day 8 when feeding activity has largely abated (Extended Data Fig. 2a), suggesting that the drugs do not act through caloric restriction. Furthermore, worm motility was preserved (Extended Data Fig. 2b, Supplementary Videos 4–6). These results suggest that global inhibition of neural excitation extends lifespan in *C. elegans*.

To explore the neural systems that mediate lifespan, we expressed a transgenic *Drosophila* histamine-gated chloride channel (HisCl1) in different neuronal populations[13]. Addition of histamine, which is not endogenously produced by worms, activates HisCl1 and inhibits neural excitation. First, we expressed HisCl1 under the control of a pan-neuronal promoter. Continuous incubation with histamine beginning on adult day 1 or day 8 significantly extended mean lifespan (Extended Data Fig. 3a, b, i). There was no effect of histamine on the lifespan of wild-type worms that did not express HisCl1 (Supplementary Table 22).

We next expressed the HisCl1 channel in glutamatergic and cholinergic neurons, the major excitatory neuronal populations in *C. elegans*. Repression of excitation in either population robustly extended lifespan whether initiated at adult day 1 or day 8 (Extended Data Fig. 3c–f, i). Expression of HisCl1 in GABAergic neurons using an *unc-47* driver extended lifespan when initiated at day 1, but reduced lifespan when initiated at day 8 (Extended Data Fig. 3g–i). GCaMP imaging showed that addition of histamine to *unc-47*: HisCl1 worms at day 1 resulted in a marked and persistent suppression of excitation in ASH neurons, which was not observed after addition at day 8 (Extended Data Fig. 3j). Thus, blockade of GABAergic neurotransmission early in adult life may result in compensatory downregulation of excitation in other neuronal populations. Taken together, these results suggest that continuous or late-life repression of neural excitation in multiple different neuronal cell populations extends lifespan in *C. elegans*.

To explore the effect of hyperexcitation on lifespan, we suppressed GABAergic neurotransmission by using RNAi, which would be predicted to be less extensive than histamine-HisCL1-mediated blockade. When worms were treated with RNAi against the GABA vesicular transporter *unc-47*, there was a robust increase in the excitation of ASH neurons and a significant reduction in lifespan (Extended Data Figure 4a, b). Thus, the effects of neurotransmission on lifespan are bidirectional; lifespan is extended by reducing excitation and shortened by increasing excitation.

Neural activity can regulate neuropeptide secretion. To address the role of neuropeptide signaling in lifespan regulation, we evaluated worms with loss-of function of the *egl-3* proprotein convertase from an *egl-3* mutation or *egl*-3 RNAi. The *egl-3* mutants exhibited significant lifespan extension (Extended Data Fig. 4c). Lifespan extension was also observed in worms treated with *egl-3* RNAi (Extended Data Fig. 4d), consistent with previous results[14]. A similar extension of lifespan was observed in a glutamatergic loss-of-function *eat-4* mutant and the synaptic transmission mutant *unc-13* (Extended Data Fig. 4c). These results suggest that both synaptic neurotransmission and peptidergic signaling contribute to lifespan regulation.

REST and the modulation of neural excitation in the aging brain

We have previously demonstrated that the transcriptional repressor REST is induced in the aging brain[15]. Genes that were downregulated in the brain in individuals with extended longevity were enriched for the canonical REST RE1 motif in all three aging cohorts (ROSMAP: P=5e-12, CommonMind Consortium: P=8e-4, Gibbs: P=1e-2) (Supplementary Tables 1,3,5). Moreover, unbiased analysis by ChIP-seq showed that REST was the most strongly implicated transcription factor in multiple ENCODE datasets (Supplementary Tables 8–11). Furthermore, the downregulated gene set was highly enriched for neuronal REST target genes (Supplementary Table 12). Expression of these downregulated genes, as well as an index of synaptic gene expression, were inversely related to REST mRNA expression (Fig. 2a, b; Extended Data Fig. 5a, b). Furthermore, nuclear REST levels were significantly elevated in prefrontal cortical neurons in centenarians relative to individuals who were 70-80 years of age (Fig. 2c). Although REST mRNA expression is upregulated in the brain during aging[15], increased REST mRNA expression did not distinguish the extended longevity versus normal aging groups based on RNA-sequencing (Supplementary Tables 1, 3). However, for a given level of REST mRNA expression, there is greater gene downregulation in the extended longevity group (Extended Data Fig. 5c, d). These results suggest that REST repressor function is upregulated in the brain in individuals with extended longevity, resulting in downregulation of genes that mediate excitation and synaptic function.

To assess the role of REST as a modulator of neural activity in the aging mammalian brain, we examined the uptake of fluorodeoxyglucose (FDG) by PET-CT in the brains of 18 month old Nestin-Cre:REST$^{lx/lx}$ (REST cKO) mice and littermate controls (Extended Data Fig. 5e)[16]. REST cKO mice showed significantly elevated cortical ^{18}FDG uptake, indicative of increased neural activity (Fig. 2d, e). Previous studies suggest that REST can modulate excitability in mouse models of epilepsy induced by kindling or kainate[16,17]. To assess excitability during aging, we performed electroencephalographic (EEG) recordings of REST cKO mice (Supplementary Table 13). Intermittent epileptiform discharges were significantly more frequent in 22-month-old REST cKO mice than in controls (Fig. 2f). Furthermore, challenge with the GABA antagonist pentylenetetrazol (PTZ) significantly increased seizure duration in REST cKO mice relative to controls (Fig. 2g), with a trend to increased mortality (Extended Data Fig. 5f). These results suggest that REST globally represses neural activity and prevents hyperexcitation in the aging brain.

Regulation of longevity and neural excitation by *C. elegans* REST orthologs

The *C. elegans* gene *spr*-4 is a structural and functional ortholog of mammalian REST that protects against toxic stressors, such as reactive oxygen species and amyloid β-protein[15]. To determine if *spr-4* modulates lifespan, we induced endogenous *spr-4* expression by utilizing the RNA-guided endonuclease Cas9 as a programmable transcription factor[18]. A nuclease-deficient variant of Cas9 (dCas9) was fused to the transcriptional activator VP16 (dCas9::VP64) and stably introduced into *C. elegans* together with four small guide RNAs (sgRNAs) targeting the *spr-4* promoter. This resulted in a modest elevation of *spr-4* mRNA and protein expression, and a significant increase in mean lifespan (Extended Data Fig. 6a–

d). Expression of dCas9::VP64 and *spr-4* sgRNAs in worms with the loss-of-function allele *spr-4*(*tm465*) did not affect lifespan, suggesting specificity for *spr-4* (Extended Data Fig. 6e). Moreover, *spr-4* overexpression robustly reduced excitation in ASH neurons (Extended Data Fig. 6f). Thus, *spr*-4 both represses neural excitation and extends lifespan.

The forkhead transcription factor DAF-16 is the central downstream target of the *daf-2*/insulin IGF-like signaling pathway that regulates lifespan in *C. elegans*. RNAi-mediated knockdown of DAF-16 prevented lifespan extension by *spr-4* overexpression (Extended Data Fig. 7a). Furthermore, lifespan extension by the neural excitation inhibitors nemadipine and ivermectin was also dependent on *daf-16*, and ivermectin elevates both total and nuclear levels of DAF-16 (Extended Data Fig. 7b–d). Thus, *daf-16* mediates lifespan extension by *spr*-4 and neural suppression.

To further explore the effects of REST orthologs on the *daf-2*/*daf-16* signaling pathway, we performed *daf-2* RNAi in wild-type, *spr-3* and *spr-4* loss-of-function mutants, and an *spr-4*;*spr-3* double mutant. As previously shown[19], *daf-2* RNAi extends lifespan by ~50% in wild-type worms. Mutations of *spr-3*, *spr-4*, or both, significantly reduced lifespan extension by *daf-2* RNAi (Extended Data Fig. 8a). Mutations in *spr-3* and *spr-4* also reduced the lifespan extension associated with the loss-of-function *daf-2*(*e1370*) allele; the greatest reduction occurred in the *spr-4;spr-3;daf-2* triple mutant (Fig. 3a). The *spr-3* and *spr-4* mutants did not affect lifespan in a wild-type background (Extended Data Fig. 8b), in contrast to a previous report that suggested a lifespan effect of *spr-3* mutants[20]. These results suggest that *spr-3* and *spr-4* contribute to the regulation of lifespan by the insulin/IGF-like signaling pathway in worms.

We next asked whether the *C. elegans* orthologs *spr-3* and *spr-4* function in neurons to regulate lifespan. To address this question, we utilized a *C. elegans* line in which RNAi was abolished by deletion of the double-stranded RNA transporter *sid-1*, but restored specifically in neurons by a *sid-1* transgene driven by a neuron-specific promoter[21]. These alleles were crossed into the *daf-2(e1370)* mutant background, and RNAi-mediated knockdown of both *spr-3* and *spr-4* was performed. Neuronal knockdown of SPR-3 and SPR-4 significantly reduced lifespan (Fig. 3b, Extended Data Fig. 8c). Thus, neuronal expression of *spr-3* and *spr-4* contributes to lifespan extension in the *daf-2* mutant.

To gain further insight into the effects of *spr-3* and *spr-4* on *daf-2* function and lifespan, we performed RNA-seq on wild-type worms and worms with mutations in *spr-4;spr-3, daf-2*, and *spr-4;3;daf*-2 (triple mutants) (Extended Data Fig. 8d; Supplementary Table 14). The comparison of triple mutant *spr-4;3;daf-2* worms with single mutant *daf-2* worms was notable for highly significant transcriptome changes in GO terms related to neural excitation, signaling and synaptic function (Fig. 3c, Supplementary Table 15). Furthermore, gene expression changes in *daf-2* mutants and *spr-4;3* mutants were overlapping (Extended Data Fig. 8e), and genes downregulated in *daf-2* mutants but upregulated in the *spr-4;3;daf-2* triple mutants were enriched for GO terms related to neural excitation (Supplementary Table 16). These results suggest that repression of neuronal genes is a conserved regulatory feature of REST and its worm orthologs.

A central question is whether SPR-3 and SPR-4 affect lifespan by suppressing neural excitation. GCaMP calcium imaging showed that neural excitation was strongly suppressed in *daf*-2 mutants both in young adult worms and during aging (Fig. 4a, b; Extended Data Fig. 8f). The *spr-4;3* mutations partially restored neural excitation in *daf-2* mutants (Fig. 4a, b, Supplementary Videos 1–3), but did not increase excitation in wild-type worms (Extended Data Fig. 8g). Suppression of excitation in *daf*-2 mutants was not mediated by neuronal DAF-16 (Extended Data Fig. 8h). However, inhibition of neural excitation with ivermectin reversed the lifespan shortening effect of *spr-4;3* mutations in *daf-2* mutant worms (Fig. 4c). Thus, SPR-3 and SPR-4 contribute to the extreme longevity of *daf-2* mutant worms by repressing neural excitation.

To identify the neural systems affected by SPR-4 and SPR-3, neurotransmitters and neuropeptides were targeted by RNAi in *spr-4;3;daf-2* triple mutants and d*af-2* single mutants. The most significant lifespan effects were observed following RNAi directed against signaling through glutamatergic (*eat-4*), cholinergic (*cha-1/unc-17*) and monoaminergic (*cat-2*) neurons, and by RNAi to axonal kinesin (*unc-104*) and the proprotein convertase (*egl-3*) (Fig. 4d, Extended data Fig. 8i). These results suggest that SPR-3 and SPR-4 suppress excitatory neurotransmitter systems, as well as neuropeptide signaling, to extend lifespan in *daf-2* mutant worms.

Loss-of-function of *daf-2* extends lifespan through activation of DAF-16[22]. Following *daf*-2 RNAi, *spr-4;3* mutants showed reduced total and nuclear DAF-16 levels (Extended Data Fig. 9a). RNA-seq analysis of day10 *spr-4;3;daf-2* triple mutant worms showed a significant reduction in the expression of DAF-16 target genes relative to *daf-2* single mutants (Extended Data Fig. 9b–d, Supplementary Tables 17, 18). Furthermore, inhibition of neural excitation by ivermectin restored DAF-16 levels in *spr-4;3* mutants following *daf-2* RNAi (Extended Data Fig. 9e). Thus, SPR-3 and SPR-4 suppress neural excitation (Fig. 4a, b), which leads to the activation of DAF-16.

REST, FOXO1 and Neural Excitation

We next asked if the association between REST, neural excitation and human longevity (Fig. 2a–c) might be mediated by a mammalian forkhead transcription factor orthologous to *C. elegans* DAF-16. REST has been shown to regulate the expression of FOXO1 in SH-SY5Y neuroblastoma cells[15]. In the human brain, REST mRNA expression was positively correlated with FOXO1 expression, but did not correlate with the expression of other FOXO family members (Fig. 5a, Extended Data Fig. 10a). Furthermore, REST and FOXO1 co-localized in neurons of the aging human prefrontal cortex (Extended Data Fig. 10b), and nuclear levels of REST and FOXO1 were strongly positively correlated in all age groups (Fig. 5b).

To determine whether REST regulates FOXO1 expression in the brain, we examined REST cKO and littermate control mice. FOXO1 localized predominantly to cortical neurons, and showed an age-related increase in 18 month old relative to 9 month old control mice (Fig. 5c). Age-dependent induction of nuclear FOXO1 was abolished in REST cKO mice (Fig.

5c). Thus, regulation of forkhead transcription factors is a conserved feature of REST and its *C. elegans* orthologs.

To explore the role of neural excitation in FOXO1 regulation, primary mouse cortical neuronal cultures were treated with kynurenic acid, a broad spectrum glutamate receptor antagonist, or with either APV or NBQX, NMDA and AMPA/kainate receptor antagonists, respectively. Kynurenic acid and NBQX significantly increased nuclear and total FOXO1 levels (Extended Data Fig. 10c). Thus, FOXO1 is regulated by glutamatergic signaling in mammalian cortical neurons, paralleling the effect of neural excitation on DAF-16 in worms.

Discussion

Here we show that extended longevity and cognitive preservation in humans is associated with coordinate downregulation of genes that mediate excitatory neurotransmission. In the model system *C.elegans*, an increase in the activity of excitatory neurons is a normal concomitant of aging. Global inhibition of neural excitation, or inhibition of specific excitatory neuronal populations, particularly glutamatergic or cholinergic neurons, resulted in robust lifespan extension. These findings are consistent with previous studies which showed that the anticonvulsants ethosuximide and valproic acid can extend lifespan in *C. elegans* [23–25]. Moreover, we found that lifespan was dynamically regulated by the excitatory-inhibitory balance of neural circuits. Thus, an imbalance between neural excitation and inhibition might degrade neural function and contribute to the aging process.

Our findings suggest that REST and the *C. elegans* orthologs SPR-3/4 regulate aging by reducing neural activity as transcriptional repressors of synaptic genes. Aging conditional REST-deficient mice exhibit increased cortical neural activity and hyperexcitability. This is consistent with previous studies in neuronal cell culture which suggest that REST maintains neural network homeostasis by buffering changes in neural excitation[26, 27].

It is intriguing that REST and neural activity converge with insulin/IGF signaling to regulate the activity of forkhead transcription factors that play pivotal roles in lifespan regulation[22,28]. The activation of *daf-16* by REST orthologs in worms and FOXO1 by REST in humans might be a mechanism for integration of neural activity with metabolism. We suggest that activating REST and reducing excitatory neural activity may be an approach to slowing aging in humans.

Materials and Methods

Brain sample procurement and description.

Postmortem human brain material was procured in accordance with institutional guidelines governed by approved protocols. Tissue samples were procured from the Rush University Medical Center and the Brigham and Women's Hospital. Tissue samples (both paraffin-embedded and frozen) from Rush University Medical Center were derived from participants in the Religious Order Study (ROS) and Rush Memory and Aging Project (MAP) at the Rush Alzheimer's Disease Center, which are longitudinal, clinical-pathologic studies of aging, cognitive decline and AD[29, 30]. Study participants agreed to comprehensive annual

clinical and neuropsychological evaluation and brain donation at death. Twenty-one cognitive function tests were employed in the present study, including a summary score of all 17 tests used as a measure of global cognition, and separate measures of episodic, semantic, and working memory, perceptual speed, and visuospatial ability. The follow-up rate exceeds 95% and the autopsy rate exceeds 90%. All autopsy cases underwent a uniform structured neuropathologic evaluation of AD, including assignment of Braak (measure of number and distribution of neurofibrillary tangles), CERAD (Aβ plaque pathology), and NIA-Reagan (composite measure of neurofibrillary tangles and amyloid plaques) scores. Paraffin-embedded brain samples were also obtained from the Brigham and Women's Hospital. These samples included young adult cases without neurological abnormalities.

Immunofluorescence analysis of human brain.

Immunofluorescence analysis using paraffin-embedded brain sections was performed in the prefrontal cortex (Broadmann areas 9, 10 and 47). Paraffin-embedded tissue sections were first deparaffinized in xylene, then rehydrated with decreasing concentrations of ethanol and placed in water. Sections then underwent antigen retrieval using the Diva decloaker (BioCare, USA). They were then washed and blocked with 2% BSA, 0.1% Triton X-100 in PBS for 1 hr at room temperature. Primary antibodies were diluted in 2% BSA, 0.1% Triton in PBS. Following overnight incubations, sections were washed three times with PBS. Secondary antibodies, diluted in 2% BSA, 0.1% Triton in PBS were either biotin-coupled (1:200, Vector Labs, USA) or coupled to Alexa fluorophores (1:300, Invitrogen). Sections were incubated with 1% Sudan Black in 80% ethanol, for 10 minutes, to suppress lipofuscin autofluorescence. Following washes in PBS, sections were mounted and imaged using confocal microscopy. The following antibodies have been used for immunolabeling studies: (i) a rabbit polyclonal IgG recognizing a region between residues 1050 and the C-terminus (residue 1097) of REST (Bethyl laboratories, IHC-00141); (ii) a goat polyclonal IgG recognizing the C-terminal region of FOXO1a (LSBio B415, discontinued, replaced with LSBio 1322). To quantify immunofluorescence, images that were randomly acquired in selected brain regions were analyzed in the Metamorph® image analysis system. Antigen-expressing areas within each neuron (such as the nucleus) were selected using the average signal intensity measured. Values were corrected by subtracting the average slide background intensity (measured outside of cells). The investigator was blinded to sample origin or diagnosis.

To assess the relationship between the levels of nuclear REST protein and FOXO1, we performed confocal immunofluorescence with triple-labeling for REST, MAP2 and FOXO1. Multiple 40x pictures were acquired (at various locations) within the prefrontal cortex displaying pyramidal neurons using an Olympus Fluoview Confocal Microscope. For cases displaying a majority of pyramidal neurons with very high (or very low) nuclear REST levels, fields were also included that displayed lower (or higher, respectively) REST levels, to test for potential correlations between REST and FOXO1. Antigen-expressing areas within neuronal nuclei were selected using the Metamorph® image analysis system and the average signal intensity was measured. Values were corrected by subtracting the average slide background intensity (measured outside of cells). Between 70 and 115 pyramidal neurons were quantified for each case.

Conditional REST-knockout mice.

Animal housing and experimental procedures were approved by the Institutional Animal Care and Use Committee of Harvard Medical School. Mice carrying floxed alleles of REST flanking exon 2 were described previously[31, 32]. These mice were crossed to Nestin-Cre transgenic mice (Jackson laboratory; strain No. 003771) to achieve REST conditional inactivation in the nervous system. The Nes-Cre transgene is in the C57BL/6J background, and the RESTlx/lx alleles were in a hybrid C57BL/6J and 129Sv/Ev background. The resulting Nestin-Cre:RESTlx/lx conditional knockout mice (hybrid C57BL/6J and 129Sv/Ev background), referred to as REST cKO, were born at expected Mendelian ratios, were viable and fertile, and did not display any visible alterations. The control group included RESTlx/lx and Nes-Cre mice. Mouse genotyping by PCR was performed using the following primers to amplify a region in the REST gene flanking exon 2: re08 (5′-CATGCGAGTACTGCCATACCCAAC-3′), re09 (5′-GTGATGGGGCAGTCTTCTGGAGG-3′), and re11 (5′-GGCACACCTTTAATCCTAGCTTC-3′); this allowed the identification of WT (220 bp), floxed (264 bp) or recombined (375 bp) REST alleles. The experimental groups included both male and female mice. The REST cKO and REST+/+ control groups were composed of littermate mice (same genetic background). Mice were identified by eartag numbers, and were randomly selected for PET/CT and EEG experiments, as well as histological processing (perfusion, brain dissection, etc.).

Immunofluorescence analysis of mouse brain.

Mice were anesthetized with isoflurane and carbon dioxide and then perfused with cold PBS buffer for 20 minutes. Brains were rapidly removed and placed in 4% PFA overnight. They were then processed for paraffin embedding, according to standard procedures. The investigator was blind to the genotype. To assess FOXO1 nuclear expression in cortical neurons, coronal brain sections from WT and REST conditional KO mice (aged 9 or 18 months) were immunolabeled with FOXO1 and MAP2 antibodies. Cortical neurons (MAP2-positive) were identified and FOXO1 mean fluorescence intensity in each nucleus was measured using the Metamorph software. Between 50-100 neuronal nuclei were assessed for FOXO1 expression, and the mean FOXO1 nuclear expression was derived for each animal. To confirm REST deficiency (Extended Data Fig. 5e), REST cKO mouse cortical sections were labeled with an anti-REST antibody provided by the Hsieh lab (see Supplementary Table 20).

PET-CT of REST cKO mice.

Mice were anesthetized with 3% isoflurane (Baxter Medical) and medical grade oxygen at a rate of 1 L/min. A CT scout scan was done first, followed by a CT scan and a dynamic PET scan. Each mouse received the same dose per gram of body weight, 1.75 Ci/g ^{18} Fluorodeoxyglucose (FDG) tracer solution by tail vein injection, followed by a 0.1 ml saline flush. Dynamic PET imaging for each mouse was immediately performed for 1 hour (in vivo PET) using a small animal PET/CT scanner (eXplore Vista; GE Healthcare). The spatial resolution of the PET scanner was 1.6 mm at the center of the field-of-view. The data were acquired in 3D mode at the energy window of 250–700 keV, which yields 4% count

sensitivity. For each timepoint, 5 or 6 3-D volumes, spanning cortical and subcortical regions, were selected in the center of the brain of the animal, with volumes of .2 cm^3 each, and used for quantification using the eXplore Vista software. Averages of these regions were used as the standard uptake value (SUV) for the animal.

Cell culture.

Primary cortical neuronal cultures, derived from E16.5 wildtype C57BL/6J fetuses, were plated in 10% serum-containing neuronal culture media (neurobasal medium containing B27 supplements, penicillin, streptomycin, and GlutaMax) on either coverslips or culture dishes that were pre-coated with poly-L-ornithine (Sigma p4957). Medium was changed 4 hours after initial plating to serum-free neuronal culture media, and then a half-medium change was performed every three days.

Electroencephalography of REST cKO mice

Electroencephalogram (EEG) Telemetry Unit Implantation—Mice were implanted with wireless telemetry units (PhysioTel ETA-F10; Data Sciences International, DSI, St. Paul, MN) under appropriate sterile technique per laboratory protocol as previously described[33, 3435, 36]. Mice were anesthetized by intraperitoneal (i.p.) injection of 100 mg/kg ketamine (Putney Vet, Portland, ME) and 10 mg/kg xylazine (Lloyd Inc, Shenandoah, IA). The transmitter was placed intraperitoneally, and electrodes were threaded subcutaneously to the cranium. After skull exposure, hemostasis, and identification of cranial sutures, bregma and lambda, two burr holes, 1 mm diameter, were drilled over the right olfactory bulb (reference) and left occipital cortex (active). The telemetry units' epidural electrodes connected to the leads of the transmitter were placed into the burr holes and secured by stainless steel skull screws. Once in place, the skull screws were covered with dental cement (Dentsply International Inc., Milford, DE). Mice were subcutaneously injected at 0 and 24 hours post-operatively with 5 mg/kg meloxicam (Norbrook Laboratories, Newry, Northern Ireland) for analgesia. After 1 week of recovery, mice were individually housed in their home cages in a 12 hour light/12 hour dark, temperature, and humidity controlled chamber with ad libitum access to food and water in preparation for recording.

Video EEG Recording, seizure induction and analysis—One-channel video-EEG was recorded differentially between the reference (right olfactory bulb) and active (left occipital lobe) electrodes after 24 h of acclimation in recording chambers. EEG (1000 Hz), core-body temperature and locomotor activity (200 Hz) signals were continuously sampled over a period of 48h along with time-registered videos. At the end of baseline EEG acquisition, all mice were provoked with a convulsive dose (40 mg/kg; i.p.) of pentylenetetrazol (PTZ; Sigma-Aldrich, Co., St. Louis, MO), a GABAA receptor antagonist, to measure seizure susceptibility and evaluate seizure thresholds[33, 36]. Mice were continuously monitored for clinical and electrographic epileptiform activity during both periods and post hoc verified by the blinded review of the video EEG. Following PTZ administration, latency to generalized tonic-clonic seizures (GTCs), number of seizures and, total duration of GTCs were recorded per mouse. Mice without seizures were assigned a time of 20 min at the end of the PTZ challenge observation period. One REST cKO mouse

was excluded from the analysis based on a febrile temperature of 40.68 °C, vs an average temperature of 34.56 ±1.48 °C for all other mice.

Immunocytochemical analysis of cultured cells.

Embryonic mouse cortical neuronal cultures described above were plated on poly-L-ornithine coated coverslips. Stocks of NBQX, APV(Tocris Bioscience Cat. No. 0190, 0106, respectively), and kynurenic acid sodium salt (Abcam, ab146693) were added to Neurobasal media and used in a half-medium change for a final concentration of 5uM kynurenic acid, 50 μM APV or 2 μM NBQX at day 10 of culture. After 24 hours, the culture media was aspirated and cells were fixed by incubation with 4% (v/v) paraformaldehyde in PBS for 20 minutes at room temperature, and permeabilized with 0.2% Triton X-100 in PBS for 15 minutes at room temperature. After a wash in PBS, cells were blocked with 4% BSA in PBS overnight at 4°C. Primary antibodies were diluted to the appropriate concentration in 4% BSA, and incubated overnight at 4°C. Cells were then washed 3 times in PBST (PBS with 0.05% Triton) for 10 minutes each, before adding fluorophore-conjugated secondary antibodies for 2 hours at room temperature. Fluorophore labeled cells were then washed in PBST, 3×10 minutes, and then mounted using Prolong Gold mounting medium with DAPI and anti-fade reagent (Invitrogen). Primary antibodies used in Figure 5d are rabbit anti-FoxO1 (Cell Signaling 2880) and chicken MAP2 (Sigma-Millipore, AB5392). Nuclei were identified by DAPI labeling, and the cellular distribution of FOXO1 labeling was quantified using Metamorph software. Cell identification parameters were optimized for scoring neuronal cultures, and then the same image analysis macro was applied to all images to generate average FOXO1 cellular intensities in MAP2-positive neurons.

C. elegans strains.

The N2 Bristol strain was used as the wild-type background for these studies. *C. elegans* strains were cultured at 20°C under standard conditions as described in Brenner[37]. The following mutations and chromosome rearrangements were used: LGI: *spr-4(by105)*[38], *spr-4(tm465)*[15], *daf-16(mu86)*[39], *hT2[bli-4(e937) qIs48] (I;III)* , *unc-13(e51)*[37]; LGIII:*daf-2(e1370)*[39] *eat-4(nj2)*[40]; LGV: *spr-1(ok2144)*[41], *sid-1(pk3321)*[42], *egl*-3*(gk238)*[43] and LGX *spr-3(ok2525)*[15]; EG7215(oxTi334 [*eft-3p*::*TdTomato*::*h2b*::*unc-54 3'UTR* + *Cbr-unc-119*(+)]). All strains, except for *spr-4(tm465)*, were provided by the Caenorhabditis Genetics Center (CGC), which is funded by the NIH Office of Research Infrastructure Programs (P40 OD010440). Worms which had not been outcrossed previously were outcrossed six times before use. See Supplementary Table 19 for a full listing of strains.

The s*pr-5* mutants exhibit transgenerational effects, including increased defects in DNA double strand break repair and germline apoptosis[44] as well as lifespan effects[45]. Although we have not fully evaluated the transgenerational phenotypes of *spr-3* and *spr-4* alleles, as a precaution, all lifespan assays were performed with worms no more than 5 generations removed from a heterozygote ancestor. To facilitate this, *spr-4* alleles were carried over the hT2 balancer described above, while *spr-3*(*ok2525*) was carried over the MosTIC[46] insertion *oxTi335*, which carries a *eft-3::tdTomato::h2b* fluorescent fusion construct integrated in the X chromosome at 4,348,071bp. Since *spr-3* is located on the X chromosome at 4,514,00 bp,

this effectively marked wildtype *spr-3*, allowing us to maintain heterozygous stocks of our double and single mutants.

The *daf-16::gfp* fusion line TJ356, bearing transgene *zIs356* [*daf-16p::daf-16a/b*::GFP + *rol-6*], was mildly anesthetized with 0.01% tetramizole and outcrossed to lab wild-type males twice, and then mated to *spr-4(by105);spr-3(ok2525)* double mutants. Double mutants bearing *zIs356* were recovered and propagated.

C. elegans RNAi.

Feeding RNAi experiments were performed at 20 °C as described in Kamath and Ahringer, 2003[47]. A feeding clone containing a full length *daf-2* cDNA was provided by Keith Blackwell. A daf-16 RNAi vector was provided by Eric Greer. Control RNAi was performed by feeding HT115 bacteria carrying the empty pL440 vector. A list of all RNAi clones used is available in Supplementary Table 20.

Enhanced neuronal RNAi was achieved as described in Calixto *et al*[21], by using *sid-1(pk3321)* mutants in which *sid-1* (a dsRNA transporter required for RNAi) is re-expressed solely in neurons via a *punc-119*:*sid-1* transgene. The animals are therefore systemically deficient in RNAi in all cell types except neurons, where RNAi is enhanced by heightened expression of *sid-1*.

Microinjection and transgenic strains.

For transgenic *C. elegans* experiments, lines were generated by microinjecting the relevant constructs into the gonads of the indicated worm strains. *Prab-3:*:mCherry (pGH8, Addgene: 19359) or pmyo-2::mCherry (pCFJ90, Addgene 19327): were used as coinjection markers. Three independent lines that demonstrated reliable transmission of the marker were propagated as described above for each experiment. Where possible, non-array segregating worms were also maintained as controls. For the dCas9::VP64 experiments, a *peft-3::dCas9VP64::tbb*-2 UTR construct was cloned using the Wormgate Gateway recombination system into the pCFJ151 MosSCI destination vector (Cloning, genotyping and plasmids). The EG6699 strain, bearing the *ttTi5605*, MosSCI integration site on chromosome II (at 8.42 MB) was raised on HT115 and microinjected as described in Frøkjær-Jensen C, *et al*[48]. Integration was confirmed by genotyping, as well as the absence of unrescued Unc- progeny. These worms were then microinjected with a cocktail of 4 sgRNAs (5ng/ul each) generated by nested overlap PCR (see Cloning, genotyping and plasmids), along with a pGH8 *myo-2::mcherry* (10ng/ul) as a marker. 3 transgenic lines from independent injections were selected. For simplicity of presentation, these are presented as merged data for lifespans and qPCR validation. For the GCaMP experiment, 2 of the lines were selected for mating and analysis.

The SPR-4::GFP reporter line was generated by microparticle bombardment using the fusion construct and bombardment protocol provided in Sarov et al. 2012[49] (see Cloning and Genotyping for additional detail).

Transcript analysis in *C. elegans*.

To analyze RNA from transgenic lines, 100 worms (24 hours post-L4) of each strain (including controls) were placed into 1.5 ml M9 buffer. For RNAi experiments 5 worms per plate were harvested in M9. Worms were washed once in M9, pelleted by centrifugation, resuspended in 200 µl Trizol, vortexed for 2 minutes and flash frozen in liquid nitrogen. Worms were then freeze-cracked by thawing in a 37°C water bath and re-freezing in liquid nitrogen. This was repeated 2 more times. After the final thaw, 100 µl of Trizol was added and the tubes were maintained at room temperature for 5 minutes. RNA was then extracted with 140 µl of chloroform, precipitated with an equal volume of 70% ethanol and transferred to an RNeasy spin column (Qiagen) and purified. Quantitative RT-PCR was performed directly from isolated RNA, using 1ng of RNA and the Qiagen One Step qPCR mix. All reactions were performed in triplicate.The ddCt method was used to analyze qRT-PCR data, and the dCt values were used for statistical analysis.

C. elegans motility assay.

Worms were treated for 24 hours with the indicated drugs, and then 150 worms were transferred to 1.5mL liquid NGM (1mM MgCl2, 1mM CaCl2, 200mM KHP04, 50mM NaCl) and washed once to remove bacterial clumps. Worms were transferred in 100ul volumes to a 96 u-shaped well plate, and assayed in the Nemametrix wMicrotracker (https://nemametrix.com/product-category/phenotyping-products/wmicrotracker/) per manufacturer instructions.

C. elegans lifespan determination and stress treatments.

Lifespan and aging experiments were performed at 20°C and on FUDR unless otherwise noted. For each genotype, 20-35 day 1 worms were transferred to NGM plates containing 100ug/ml FUDR. Worms were scored for viability every day or every other day, and transferred to fresh plates between day 10 and day 14. For *daf-2* mutant worms, worms were moved again at day 20-24. For histamine and ivermectin experiments, where the same plates were used for the entirety of the lifespan, a wetted towel was placed in the container with the plates to mitigate evaporative loss of water from the plates. For lifespan experiments in which untreated worms were transferred to the treatment group (e.g. day 8 histamine treatment), control worms (+/−) treatment were also transferred to fresh plates of the same type to control for any lifespan effects resulting from plate transfer. The presence or absence of FUDR is indicated for each experiment in Supplementary Table 22

For all lifespans and stress resistance experiments, worms that burst (interior leaking out through the vulva) or bagged (interior hatching of progeny) were discarded from the plate and not used in lifespan analysis, along with animals that crawled off the plate during the course of the assay. Plates with mold or other contamination were discarded.

Quantification of DAF-16::GFP fluorescence.

For quantification of GFP fluorescence in fixed animals, 25-30 worms were transferred to an Eppendorf tube containing M9 buffer, washed once in M9 and pelleted. The supernatant was removed and the pellet was frozen in liquid nitrogen. The day before imaging, worm pellets were thawed in PBS with 4% paraformaldehyde (ThermoFisher) and fixed for 30 minutes at

room temperature while rocking. The PFA was removed by washing twice with PBS, with .025% Triton (PBST, to prevent sticking), and the worms were stained with DAPI for 10 minutes at room temperature. The DAPI was removed with a final wash in PBST, and the pellet was resuspended in 15ul of ProLong Gold mounting media (Life Technologies). The worms were transferred, in 12.5ul of mounting media, to a slide, and gently placed under a coverslip, which was then sealed with clear nail polish (E.M.S.).

Slides were imaged on an Olympus Fluoview 1000 confocal microscope, using manufacturer settings for GFP and DAPI (488 and 405 laser, respectively) within 2 weeks of mounting, and all slides compared with each other were imaged on the same day, in the same imaging session. Worms were imaged via a 40x objective with a 2x digital zoom. For every worm, Z-stack image series were taken at 2 μm step sizes (roughly 13-15 images per series). To quantify nuclear GFP levels, these Z-stacks were opened in ImageJ (NIH) and flattened using a maximum intensity Z-stack projection. For pharyngeal nuclei, 3 regions of interest (ROI) were selected based on DAPI staining of nuclei, on either side of the pharynx and behind it, encompassing the bulk of the nuclei in that area. These were then used as the ROIs within which to measure GFP fluorescence, using the ImageJ intensity measuring tool. Average scores from the ROIs were computed for each worm. For Extended Data Figure 6b middle panel, Extended Data Figure 7d right panel, and Extended Data Figure 9a right panel, all nuclei located in the middle 3 z planes of the worm were individually selected using the same ROI/Intensity measuring tools. These nuclei were then used to calculate an average score per worm.

GCaMP imaging in *C. elegans*.

Data acquisition.—GCaMP imaging was performed in lines bearing *kyIs602* [sra-6::GCaMP3.0, 75 ng/μL+unc-122::GFP, 10 ng/μL], which expresses predominately in the ASH neurons. Worms were removed from plates and mounted on 7.5% agarose pads in NGM liquid media (1mM $MgCl_2$, 1mM $CaCl_2$, 200mM KH_2P04, 50mM NaCl), mixed 1:1 with .05 micron polystyrene beads (Polysciences, Inc, cat#: 08691) as described here: http://wbg.wormbook.org/2009/12/01/agarose-immobilization-of-c-elegans/. A coverslip was very gently applied and worms were imaged for a maximum of 30 minutes after mounting. Videos of 144 seconds (240 frames, ~.6 frames per second) were recorded on the confocal microscope described above (FV1000), with the confocal aperture widened to 250 microns to allow lower excitation intensity and mitigate z-drift. Worms were imaged with factory GFP settings and the 488 laser set to 2% . Videos were opened and played in Image J, and excitation events were scored by manually for Figure 4a. Scoring was performed blinded to genotype.

Analysis of GCaMP intensity changes.—For analyses of dF/F0 maximum intensity, videos were analyzed using a custom MATLAB script, which automatically registered and segmented the ASH neuron and recorded GCaMP fluorescence intensity for each frame. Videos of tracked neurons were manually reviewed and neurons that were poorly tracked were excluded from analysis. To normalize the fluorescence intensity per worm we used dF/F0 which was calculated as (F(t)-F0)/F0 where F(t) is the fluorescence intensity at time t and F0 represents an estimate of the baseline fluorescence which was calculated as the 0.2

quantile fluorescence per worm. dF/F0 max intensity was the maximum dF/F0 over the entire recording (240 frames). For analysis of nemadipine treated worms and for worms expressing the HisCL channel (and their controls), ROIs were hand-drawn because the tracking program failed due to either low signal intensity (nemadipine treated worms) or the inability to distinguish a confounding GFP signal (HISCL::GFP worms). Some worms were used in multiple GCaMP analyses.

C. elegans cloning and genotyping.

The SPR-4::GFP fusion fosmid used in bombardment (ED Fig 6a,b; Clone: 3167840880351681 C09) was provided by the Transgenome consortium (Sarov, 2012)[49]. All primers used for genotyping can be found in Supplementary Table 22.

Human brain gene expression cohorts.

ROSMAP cohort.—Brain samples were from the dorsolateral prefrontal cortex of 638 individuals spanning the range of cognitive function from cognitively normal to MCI to AD from the ROS and MAP cohorts. https://www.synapse.org/#!Synapse:syn3219045

CommonMind Consortium cohort.—Brain samples were from the dorsolateral prefrontal cortex of 602 individuals with Schizophrenia, Bipolar disease, and control individuals with no neuropsychiatric disorders. https://www.synapse.org/#!Synapse:syn2759792

Gibbs cohort.—Brain samples were from the frontal cortex of 146 neurologically normal Caucasian individuals[11].

RNA library preparation and sequencing.

Human RNAseq.—*ROSMAP cohort* https://www.synapse.org/#!Synapse:syn3388564.

CommonMind Consortium cohort. https://www.synapse.org/#!Synapse:syn3157743.

C. elegans day 2.—Libraries were prepared using Illumina TruSeq Stranded mRNA sample preparation kits from 500 ng of purified total RNA according to the manufacturer's protocol. The finished dsDNA libraries were quantified by Qubit fluorometer, Agilent TapeStation 2200, and RT-qPCR using the Kapa Biosystems library quantification kit according to manufacturer's protocols. Uniquely indexed libraries were pooled in equimolar ratios and sequenced on an Illumina NextSeq 500 with paired-end 75 bp reads by the Dana-Farber Cancer Institute Molecular Biology Core Facilities.

C. elegans day 10.—cDNA was synthesized Clontech SmartSeq v4 reagents from of 2ng RNA, due to low yields from aged worms. Full length cDNA was fragmented to a mean size of 150bp with a Covaris M220 ultrasonicator and Illumina libraries were prepared from 2ng of sheared cDNA using Rubicon Genomics Thruplex DNAseq reagents according to manufacturer's protocol. The finished dsDNA libraries were quantified by Qubit fluorometer, Agilent TapeStation 2200, and RT-qPCR using the Kapa Biosystems library quantification kit. Uniquely indexed libraries were pooled in equimolar ratios and sequenced

on Illumina NextSeq500 run with paired-end 75 bp reads at the Dana-Farber Cancer Institute Molecular Biology Core Facilities. One sequenced sample consisted of primarily ribosomal RNA and was discarded. This sample was reprocessed along with two other previously sequenced samples (as quality controls) with a new library preparation and sequencing. On a principal components plot these three samples showed no clear batch effect compared to the other samples so the resequencing of the sample that was problematic in the original batch was used. The two additional resequenced samples used for quality control were not used in the analysis.

Human sample selection and outlier analysis.

ROSMAP cohort.—Samples were excluded if missing cognitive diagnosis (cogdx) or PMI, if the expression of sex-specific genes did not agree with reported sex, or if RNA integrity (RIN)<6.5. Of the 638 samples with RNA sequencing we removed 3 due to missing information, 180 due to low RIN, 1 due to sex mismatch, and the remaining 1 sample from sequencing batch 7 the samples of which had a strong batch effect on principal components plots and were removed due to low RIN. Next we performed outlier analysis (see below), and removed 10 outliers (3 no cognitive impairment (NCI), 1 mild cognitive impairment (MCI), 5 AD dementia, 1 other dementia). After quality control, there were 443 individuals for analysis (150 NCI, 118 MCI, 164 AD dementia, 11 other dementia).

CommonMind Consortium (CMC) cohort[10].—We excluded the 10 outlier samples identified in the original publication. No other samples were removed. After quality control, of the 602 samples with RNA sequencing, there were 592 individuals for analysis (279 Control, 258 Schizophrenia, 47 Bipolar, 8 Affective/mood disorder).

Gibbs cohort.—No samples were removed due to missing information or incorrect sex. Next we performed outlier analysis, and removed 2 outliers. After quality control, there were 144 individuals for analysis.

Outlier analysis.—Outlier analysis was performed for each cohort in an iterative manner using only genes expressed in the youngold and oldestold groups at each iteration (see sections “Gene expression sample groups for human cohorts” and “Gene expression normalization and covariate adjustment”). For ROSMAP and CommonMind Consortium cohorts we used edgeR TMM-normalized log(CPM) expression. For Gibbs cohort we used log2 expression. At each iteration, the sample deemed to be the strongest outlier was removed, if any, and the process was iterated until no outliers were detected. Outlier detection was performed using principal components analysis, agglomerative hierarchical clustering using the Euclidean distance metric and average linkage criterion, and pairwise correlation of gene expression per sample. Samples were classified as outliers if they were isolated on a plot of the first and second principal components or in the hierarchical clustering tree, and had relatively low correlation with other samples determined as its mean pairwise correlation with other samples more than 3 standard deviations below the mean.

RNA sequencing read alignment and quantification of gene expression.

ROSMAP cohort.—BAM files containing reads aligned to hg19 were obtained from synapse (https://www.synapse.org/#!Synapse:syn3388564). Reads were obtained from these BAM files using Picard v1.138 (http://broadinstitute.github.io/picard/) SamToFastq. Reads were aligned to GRCh38 with Ensembl GRCh38.86 gene models using STAR version 2.5.2b[50] with options --outFilterMismatchNoverLmax 0.04 --outFilterMismatchNmax 999 --alignSJDBoverhangMin 1 --alignSJoverhangMin 8 --outFilterMultimapNmax 20 --outFilterType BySJout --alignIntronMin 20 --alignIntronMax 1000000 --alignMatesGapMax 1000000. Expression levels of genes were quantified as gene counts using FeatureCounts v1.5.1[51] with options -C -p -B -s 2 -t exon -g gene_id.

CommonMind Consortium cohort.—Gene counts were obtained from synapse. https://www.synapse.org/#!Synapse:syn3346749

C. elegans day 2 and day 10.—Quality control of sequencing reads was performed with FastQC (https://www.bioinformatics.babraham.ac.uk/projects/fastqc/). Reads were aligned to the *Caenorhabditis elegans* WBcel235 genome with Ensembl WBcel235.86 gene models using STAR version 2.5.2b with options --outFilterMismatchNoverLmax 0.04 --outFilterMismatchNmax 999 --alignSJDBoverhangMin 1 --alignSJoverhangMin 8 --outFilterMultimapNmax 20 --outFilterType BySJout --alignIntronMin 15 --alignIntronMax 1000000 --alignMatesGapMax 1000000. Expression levels of genes were quantified as gene counts using FeatureCounts v1.5.1 with options -C -p -B -s 2 -t exon -g gene_id for day 2 and -C -p -B -s 0 -t exon -g gene_id for day 10. Data are available in the Gene Expression Omnibus (GEO) under accession number GSE123146.

Gene expression sample groups for human cohorts and *C. elegans*.

ROSMAP cohort.—ROSMAP was our discovery cohort. Based on hierarchical clustering of age-associated genes (see section “Hierarchical clustering to select age group cutoffs”) we partitioned NCI individuals into 3 age groups: youngold (28 individuals, ages ≥70 and ≤80), middleold (33 individuals, ages >80 and <85), and oldestold (89 individuals, ages 85-101). Individuals with cognitive impairment were grouped into a separate cognitive impairment group (293 individuals).

CommonMind Consortium cohort.—CommonMind Consortium was a replication cohort for the ROSMAP results. We partitioned control individuals into 4 age groups: young (105 individuals, ages ≥17 and ≤60), youngold (96 individuals, ages ≥60 and ≤80), middleold (19 individuals, ages >80 and <85), oldestold (59 individuals, ages ≥85 and 90+; in this cohort, age of death greater than 90 years is censored to 90+.) Individuals with neuropsychiatric illnesses were grouped into a separate group (313 individuals).

Gibbs cohort.—Gibbs was a replication cohort for the ROSMAP results. We partitioned cognitively normal individuals into 4 age groups: young (104 individuals, ages ≥15 and <55), youngold (18 individuals, ages ≥55 and ≤80), middleold (3 individuals, ages >80 and <85), and oldestold (19 individuals, ages 85-101).

Throughout the paper, “individuals with extended longevity” refers to individuals in the oldestold groups defined above.

C. elegans day 2 and day 10.—There were 4 genotypes of worms: *daf-2*, *daf-2; spr-4;3*, N2, and *spr-4;3*, and each genotype had 3 biological replicates. Each genotype was considered as a separate group for analysis.

Gene expression normalization and covariate adjustment.

ROSMAP cohort.—Gene counts were input to edgeR[52]. Genes were deemed expressed if ≥10 individuals in a combined youngold and oldestold group had ≥ 1 counts per million (CPM). Genes not satisfying these criteria were removed keeping the original library sizes. These were expressed genes used during each iteration of outlier analysis. After outlier analysis, of 58051 annotated genes this filtering retained 18511 expressed genes for analyses involving the ROSMAP cohort. Counts were then normalized using the TMM method in edgeR. Finally, log(CPM) values were calculated for analyses other than differential expression.

To adjust gene expression for covariates we fit the linear regression model for each gene separately using lm() in R: gene expression ~ group + covariates where gene expression is log(CPM), and using the group and covariates for ROSMAP. For ROSMAP group was a factor with 4 levels: youngold, middleold, oldestold, and cognitivedecline with cognitivedecline as the reference level. The covariates were sex (factor, 2 levels), RIN (continuous), RIN^2 (continuous), PMI (continuous), and sequencing batch (factor, 8 levels). The final normalized and adjusted gene expression values were derived from adding the regression residuals to the estimated effect of the group level to preserve the effect of the group on expression. These normalized and adjusted gene expression values were used to perform gene-gene regression analysis, gene-gene group regression analysis, and visualize gene expression.

CommonMind Consortium cohort.—Gene counts were input to edgeR. Genes were deemed expressed if ≥10 individuals in a combined youngold and oldestold group had ≥ 1 counts per million (CPM). Genes that did not satisfy these criteria were removed maintaining the original library sizes. These were expressed genes used during each iteration of outlier analysis. After outlier analysis, of 56632 annotated genes, this filtering retained 19453 expressed genes for analyses involving the CommonMind Consortium cohort. Counts were then normalized using the TMM method in edgeR. Finally, log(CPM) values were calculated for analyses other than differential expression. To adjust gene expression for covariates we fit the linear regression model for each gene separately using lm() in R: gene expression ~ group + covariates where gene expression is log(CPM), and using the group and covariates for CommonMind Consortium. For CommonMind Consortium group was a factor with 5 levels: young, youngold, middleold, oldestold, and neuropsychiatric illness with neuropsychiatric illness as the reference level. The covariates used were selected from those used in the original publication: sex (factor, 2 levels), RIN (continuous), RIN^2 (continuous), PMI (continuous), clustered batch (factor, 9 levels), and Institute (factor, 3 levels). The final normalized and adjusted gene expression values were derived from adding

the regression residuals to the estimated effect of the group level to preserve the effect of the group on expression. These normalized and adjusted gene expression values were used to perform gene-gene regression analysis, gene-gene group regression analysis, and visualize gene expression.

Gibbs cohort.—Gene expression data measured on the Illumina humanRef-8 v2.0 expression beadchip platform was downloaded from NCBI GEO GSE15745. Raw intensity values for each probe were transformed using the rank invariant normalization method by the authors[11], and then log2 transformed for analysis. Probes were deemed expressed if ≥10 individuals in a combined youngold and oldestold group had Detection P-value<0.01. Unmapped probes according to updated GPL annotation were removed. These were expressed probes used during each iteration of outlier analysis. After outlier analysis, of 22184 probes this filtering retained 13239 expressed probes for analyses involving the Gibbs cohort.

To adjust gene expression for covariates we fit the linear regression model for each gene separately using lm() in R: probe expression ~ group + covariates where probe expression is log2 expression, and using the group and covariates for Gibbs. For Gibbs group was a factor with 4 levels: young, youngold, middleold, and oldestold with young as the reference level. The covariates were sex (factor, 2 levels), PMI (continuous), and prep hybridization batch (factor, 7 levels). The final normalized and adjusted probe expression values were derived from adding the regression residuals to the estimated effect of the group level to preserve the effect of the group on expression. These normalized and adjusted probe expression values were used to visualize probe expression.

C. elegans day 2 and day 10.—Gene counts were input to edgeR. Genes were deemed expressed if ≥3 samples had ≥ 1 counts per million (CPM). Genes not satisfying these criteria were removed keeping the original library sizes. Of 46739 annotated genes this filtering retained 12981 expressed genes for analyses involving *C. elegans* day 2 and 15154 expressed genes for analyses involving *C. elegans* day 10. Counts were then normalized using the TMM method in edgeR. Finally, log(CPM) values were calculated for analyses other than differential expression. For day 2 covariate adjustment was not necessary because there were no other covariates beyond the group variable. For day 10 we did not include a batch covariate because there was no observed batch effect on a principal components plot, and results were similar if a batch covariate was included and the two dropped technical repeat sequencings were used instead of their original sequenced reads (data not shown). Thus, covariate adjustment was not necessary because there were no other covariates beyond the group variable. These normalized gene expression values were used to visualize gene expression.

To visualize differentially expressed genes in heat maps, normalized gene expression values were transformed to a z-score per gene and thresholded to [−3, 3].

Differential expression analysis.

ROSMAP cohort.—Differential expression analysis between the oldestold and youngold groups with covariate adjustment using the covariates listed in section “Gene expression

normalization and covariate adjustment: ROSMAP" was performed for expressed genes using edgeR (estimateDisp, glmFit, and glmLRT with default arguments) in R. All 443 samples were included to increase statistical power during covariate modeling. Genes were considered differentially expressed if Benjamini and Hochberg false discovery rate (FDR) was ≤0.1, which was calculated using the R function p.adjust with argument method="fdr"[53].

CommonMind Consortium cohort.—Differential expression analysis between the oldestold and youngold groups with covariate adjustment using the covariates listed in section "Gene expression normalization and covariate adjustment: CommonMind Consortium" was performed for expressed genes using edgeR (estimateDisp, glmFit, and glmLRT with default arguments) in R. All 592 samples were included to increase statistical power during covariate modeling. Genes were considered differentially expressed if FDR≤0.05 and absolute value of the fold change ≥ 1.2.

Gibbs cohort.—Differential expression analysis between the oldestold and youngold groups with covariate adjustment using the covariates listed in section "Gene expression normalization and covariate adjustment: Gibbs" was performed for expressed probes using linear regression models in limma (lmFit and eBayes with default arguments) in R. All 144 samples were included to increase statistical power during covariate modeling. Probes were considered differentially expressed if FDR≤0.05.

C. elegans day 2 and day 10.—Differential expression analysis between all pairs of groups such as *spr-4;3;daf-2* vs *daf-2* was performed for expressed genes using edgeR (estimateDisp, glmFit, and glmLRT with default arguments) in R. All 12 samples were included during edgeR analysis. Genes were considered differentially expressed if FDR≤0.05.

Gene sets and gene set enrichment analysis.

Gene annotation and gene sets used for functional gene classification into biological process (BP), molecular function (MF), and cellular component (CC) were from the GRCh38.p7 database downloaded from Ensembl Biomart on November 2, 2016.

Synaptic transmission genes were genes that had direct or indirect annotation of GO Biological Process "chemical synaptic transmission" GO:0007268.

REST target genes. The REST RE1 motif position-specific weight matrix MA0138.2 was obtained from JASPAR[54]. FIMO version 4.10.1[55] was used with the Homo sapiens genome sequence GRCh38 to predict REST binding sites. A gene was defined to be a REST target if it had an RE1 motif with motif P-value < 1e-7 that was +/−10kb from the transcription start site of any transcript of the gene in the Ensembl GRCh38.86 gene models. This procedure identified 2632 REST target genes before filtering for expressed genes in each cohort during gene set enrichment analysis.

ENCODE ChIP-seq transcription factor target gene sets were from the ENCODE_TF_ChIP-seq_2015 database[56] downloaded from http://amp.pharm.mssm.edu/Enrichr/ on March 8, 2018.

Cell type analysis gene sets were derived from a transcriptome database of the major cell classes of the mouse cerebral cortex[57] using data from https://web.stanford.edu/group/barres_lab/brain_rnaseq.html. To select cell marker genes first we calculated the fold expression of each gene in each cell type by dividing the FPKM expression in that cell type by the mean of the FPKM expression in the other 6 cell types. For each cell type we selected as cell marker genes those that had at least 10-fold higher expression and that had one-to-one human-mouse homologs. Homologs were downloaded from http://www.informatics.jax.org/downloads/reports/HOM_MouseHumanSequence.rpt on November 16, 2016.

DAF-16 class I (upregulated) genes were derived by selecting genes with FDR<0.01 and class="up" from Tepper *et al* Table S1[58].

For gene set enrichment analysis of differentially expressed genes, we only retained genes in each gene set that were expressed in that differential expression analysis. Gene set enrichment analysis was performed separately for upregulated genes vs not upregulated genes, downregulated genes vs not downregulated genes, and differentially regulated genes vs not differentially regulated genes. For Gene Ontology gene sets, gene set enrichment was determined using the topGO R package[59] using the classic algorithm and Fisher's statistic. Gene set enrichment for REST target genes, ENCODE ChIP-seq transcription factor target gene sets, and Cell type analysis gene sets was performed using the hypergeometric distribution (one-tailed). Gene sets with less than 5 genes after filtering for expressed genes were removed before the gene set enrichment false discovery rates were calculated.

To calculate the statistics for overlap of *daf-2* upregulated genes, *spr-4;3;daf-2* upregulated genes, *spr-4;3;daf-2* downregulated genes, and daf-16 class I genes for *C. elegans* day 10 we used the SuperExactTest version 1.0.0 R package[60].

For meta-analysis of GO terms and ENCODE ChIP-seq transcription factor target gene set enrichment from the ROSMAP, CMC, and Gibbs cohorts, we used Stouffer's method with weights[61] for combining p-values implemented in the sumz function in the metap R package[62]. P-values equal to 1 were replaced with 0.999999 to comply with the requirement that 0<P-value<1. For study weights we used the square root of the total number of individuals in the combined youngold and oldestold group for each study (ROSMAP, sqrt(117); CMC, sqrt(155); Gibbs, sqrt(37)[63].

Hierarchical clustering to select age group cutoffs.

Normalized and adjusted gene expression values were derived as described in the section "Gene expression normalization and covariate adjustment" with the following changes. First, the group variable was a factor with levels cogdx1, cogdx2, cogdx3, cogdx4, cogdx5, and cogdx6 (ROSMAP); control, Schizophrena, Bipolar, Affective (CommonMind Consortium); or not included (Gibbs). Next, genes were deemed expressed if ≥10 individuals in the

cognitively normal group (ROSMAP, cogdx1; CommonMind Consortium, control with age>=60) had ≥ 1 counts per million (CPM). Genes not satisfying these criteria were removed keeping the original library sizes. For the Gibbs cohort, probes were deemed expressed if ≥10 individuals with age>=55 had Detection P-value<0.01 and no samples had NA values. Probes not satisfying these criteria were removed. These were expressed genes used for analysis. This filtering retained: ROSMAP, 18734 expressed genes; CommonMind Consortium, 19615 expressed genes; Gibbs, 13411 expressed probes. For RNA-seq data, counts were then normalized using the TMM method in edgeR, and log(CPM) values were calculated for expression. Finally, age was included as a continuous covariate, and the effects of group and age were added back to the residuals. Then cognitively normal aged individuals were selected in each cohort (ROSMAP, cogdx1; CommonMind Consortium, control with age≥60; Gibbs, age ≥55). To determine age-associated genes, the expression of each expressed gene was correlated with the age of death of the individual using spearman correlation. Genes with spearman rank correlation FDR<0.1 (ROSMAP, n=1025 genes) or FDR<0.05 (CommonMind Consortium, n=6828 genes; Gibbs, n=203 probes) were age-associated genes. Permuting sample ages before calculating the spearman correlations gave no genes passing the FDR threshold. Genes were then normalized to have mean 0 and standard deviation 1 across individuals, and genes with normalized expression >=3 or <=−3 were set to 3 or −3, respectively. The Pearson correlation coefficient between individuals was then calculated using only age-associated genes.

Agglomerative hierarchical clustering using the Euclidean distance metric and average linkage criterion was performed on the matrix of pair-wise Pearson correlations to cluster individuals. The resulting tree was cut into 3 groups, and the distribution of the age of death of individuals of each group was analyzed. Using the ROSMAP cohort, for the cluster with the smallest median age, with c1 individuals, we calculated the number of individuals, nyoc, with age of death in [70, youb], of nyo total, and for the cluster with the largest median age, of c2 individuals, we calculated the number of individuals, nooc, with age of death in [oolb, Inf), of noo total, as the age boundaries youb and oolb varied. For each set of age cutoffs we assigned a score as (nyoc/nyo*c1 + nooc/noo*c2)/(c1+c2). To ensure adequate sample sizes for differential expression and because individuals with older ages appeared more heterogeneous in the cluster heat map we only considered age cutoffs with at least 25 individuals in the youngold group and at least 75 individuals in oldestold group. Based on the top scoring age cutoffs in the ROSMAP cohort, we selected youb=80 and oolb=85. Thus, the age cutoffs for defining the youngold, middleold, and oldestold groups used for differential expression in the ROSMAP, CommonMind Consortium, and Gibbs cohorts were selected to be ≤80, >80 and <85, and ≥85, respectively.

Statistical analysis and data representation.

Statistical analysis was performed using R. Statistical tests used are noted in the figure legends or in the relevant Methods section. Throughout the paper, all tests are two-sided and unpaired unless stated otherwise. A significance level of 0.05 was used to reject the null hypothesis unless stated otherwise.

Boxplots throughout the paper show the median, lower and upper hinges (first and third quartiles), upper whisker (hinge to the largest value no further than 1.5 * IQR from the hinge), lower whisker (hinge to the smallest value at most 1.5 * IQR of the hinge), and outlying points beyond the whiskers. Additionally, all points are plotted on top of the boxplot and randomly jittered horizontally

A t-test was used for parametric comparisons between two groups with normally distributed data, and utilized t.test(). For groups with equal variance Student's t-test was used (argument var.equal=TRUE); otherwise Welch's t-test was used (argument var.equal=FALSE). ANOVA was used for parametric comparisons between more than two groups and used aov(). The Mann–Whitney U test was used for nonparametric comparisons between two groups without knowledge of their distribution and used wilcox.test() with arguments exact=TRUE, correct=FALSE. Levene's test was used to investigate the homogeneity of variance across groups and used leveneTest() from the "car" R package. Q-Q plots and the Shapiro-Wilk test were used to assess normality and used shapiro.test(). The Bonferroni outlier test was used to assess outliers and used outlierTest() from the "car" R package. The log-rank test was used to compare the survival distributions of two groups. Survival statistics were calculated using survfit() with argument type="kaplan-meier" and survdiff(). To determine if there was a linear relationship between two variables we fit a linear regression model and tested the null hypothesis that the slope of the regression line is 0 using a two-sided t-test using lm(). P-values were corrected for multiple comparisons where noted using p.adjust() with argument method="fdr", "holm", or "bonferroni" for false discovery rate, Holm's method, or Bonferroni correction, respectively. The GCaMP imaging data indicated that nonparametric analyses were most appropriate and thus were used for all GCaMP analyses. In Fig 2e the presence of candidate outliers and/or potential non-normality for timepoints 1-12.5 minutes suggested a Mann–Whitney U test was more appropriate although a t-test produced similar conclusions. Meta-analysis of lifespan experiments that performed pairwise comparisons among more than 2 groups (Extended Data Fig. 8a right, Extended Data Fig. 8c) used pairwise Student's t-tests implemented in pairwise.t.test() with argument pool.sd=TRUE to calculate a common standard deviation used for all groups and comparisons.

Extended Data

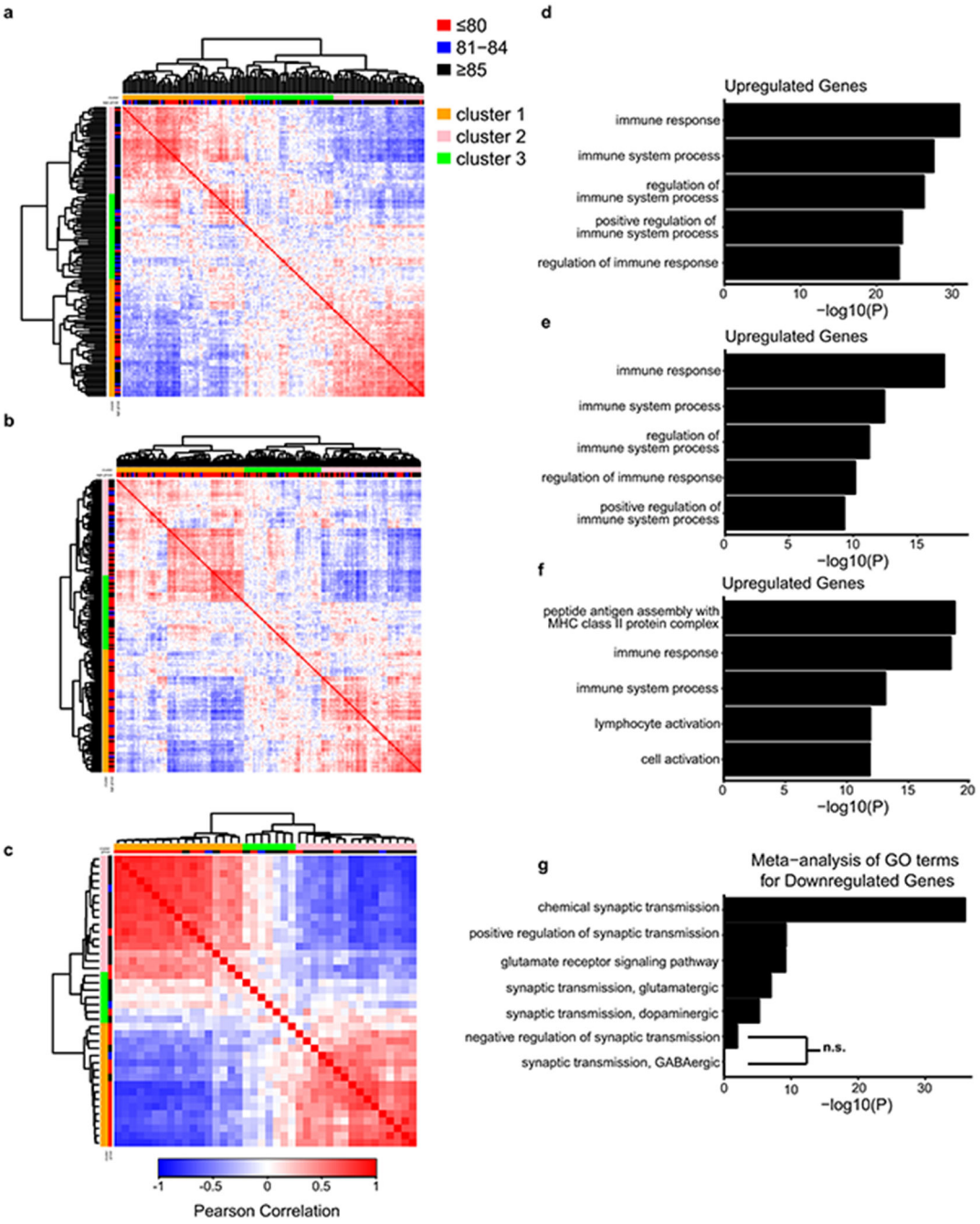

Extended Data Figure 1. Partitioning of the aging human population for analysis of gene expression in the brain.

a-c, Adjusted gene expression profiles for age-associated genes were compared between cognitively normal aged individuals to derive a matrix of Pearson correlation coefficients that indicate the degree of similarity between any two cases in the ROSMAP (a, dorsolateral prefrontal cortex, n=150 individuals) CommonMind Consortium (b, dorsolateral prefrontal cortex, n=174 individuals) and Gibbs (c, frontal cortex, n=40 individuals) cohorts. **d-f**, Most significantly enriched GO terms for upregulated genes in the cortex of cognitively normal

individuals who lived to be ≥85 years old relative to individuals who lived to be ≤80 years old in the ROSMAP (d, n=117 individuals), CommonMind Consortium (e, n=155 individuals), and Gibbs (f, n=37 individuals) cohorts. P-values were calculated using Fisher's exact test (see Methods). **g**, Meta-analysis of GO term enrichment for downregulated genes. Shown are selected GO terms related to excitatory and inhibitory synaptic transmission. The individual cohort enrichment p-values were combined using Stouffer's method (see Methods). NS, FDR>0.1.

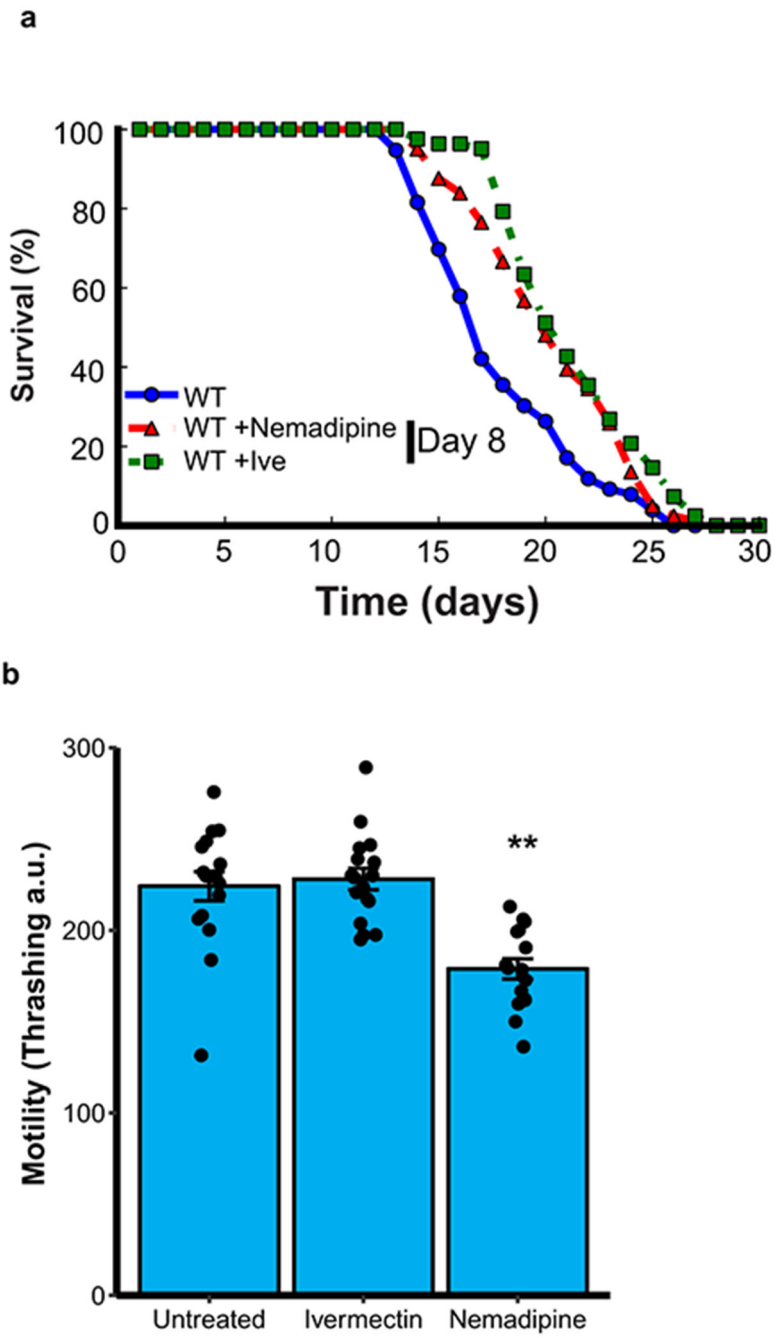

Extended Data Figure 2. Ivermectin and nemadipine extend lifespan without interfering with worm motility.

a, Worms were transferred at day 8 to either standard NGM plates or plates containing ivermectin (1 pg/ml) or nemadipine (2 μM). Shown is a representative curve of an experiment repeated twice. Nemadipine versus WT: P=3.2 e-4; Ivermectin versus WT: P=2.2e-7 by log-rank test. Nemadipine, n=81; Ivermectin, n=82; WT, n=76. **b.** Day 2 worms treated with nemadipine or ivermectin for 24 hours were transferred to liquid culture and thrashing rate was assessed using the Nemametrix wMicrotracker (see Methods). Shown are

mean motility scores for the first 60 minutes, ± S.E.M.. Untreated, n=17 wells; Ivermectin, n=17 wells; Nemadipine, n=16 wells. Each well contained ~10 worms. **P=1.7e-4 vs untreated, Mann–Whitney U test with multiple testing correction by Holm's method. Results are representative of an experiment replicated twice.

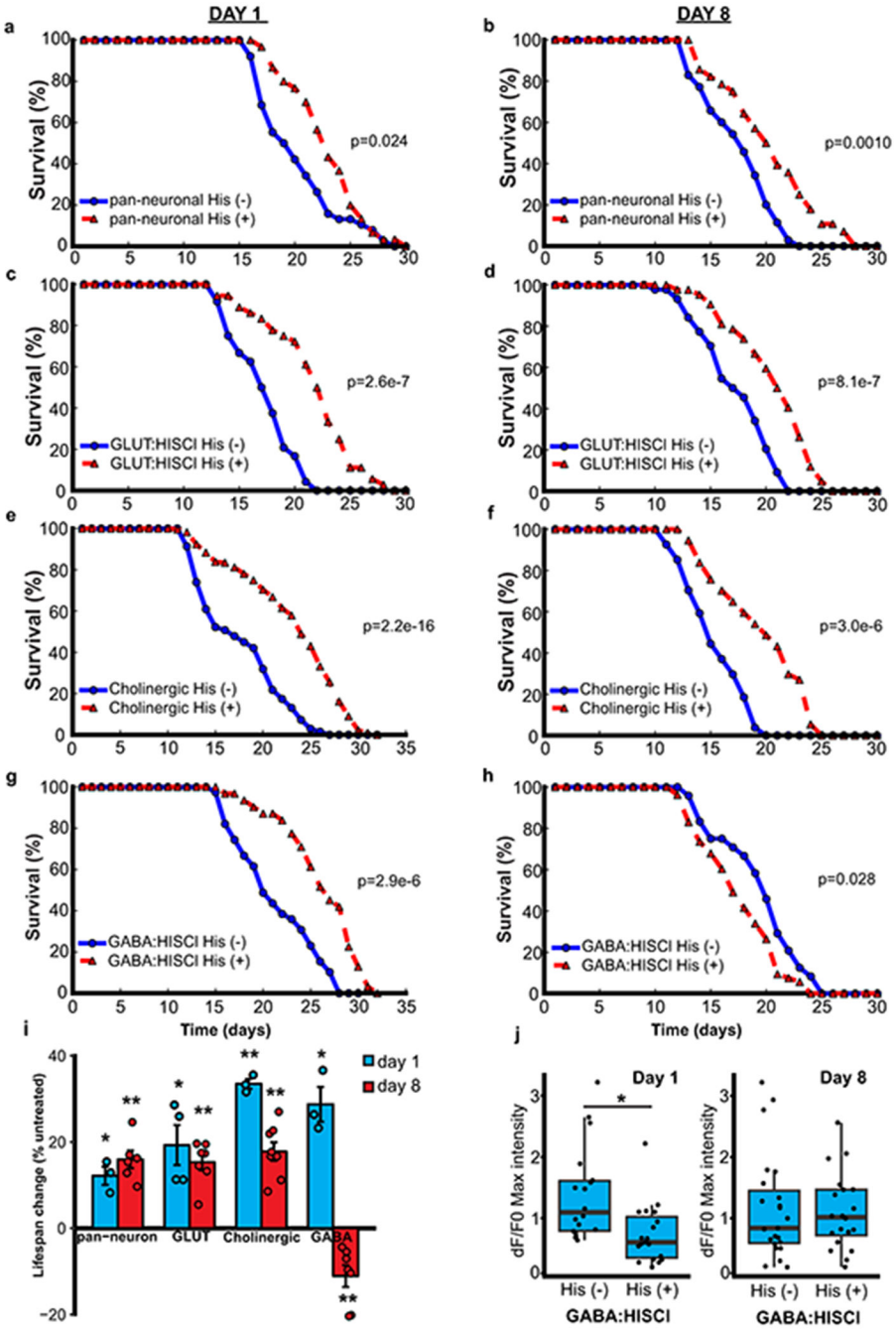

Extended Data Figure 3. Repression of multiple neurotransmitter systems extends lifespan in *C. elegans*.

a-h. *C. elegans* lines expressing the transgenic HisCl1 channel in the indicated neuronal populations were treated with 10 mM histamine (His+) starting at adult day 1 (a, c, e, g) or day 8 (b, d, f, h) and compared to untreated controls (His−). P-values are by log-rank. See Supplementary Table 22 for individual n values and statistics. **i,** Shown is the mean lifespan extension ± S.E.M. for worms treated with histamine at days 1 or 8 relative to untreated controls for at least three independent replicates, *P<0.05, **P<0.01 by Student's *t*-test.

HisCl1was driven using the GAL4SK:VP64 system for the GABAergic (GABA), glutamatergic (GLUT) and cholinergic systems, using *unc-47*, *eat-4*, and *unc-17* drivers, respectively (see Supplementary Table 19 for details). **j,** Reduced ASH neuron excitation following inhibition of GABA activity at day 1 but not day 8. Shown is normalized maximum GCaMP fluorescence in day 1 and 8 *unc-47*:HisCl1 worms that were treated with 10 mM histamine [His (+)] on the indicated day, or untreated controls [His (−)]. Day 1 His(−): n=18 worms; Day 1 His(+), n=19 worms; Day 8 His(−): n=23 worms; Day 8 His(+): n=20 worms. *P=1.1e-3 by the Mann–Whitney U test.

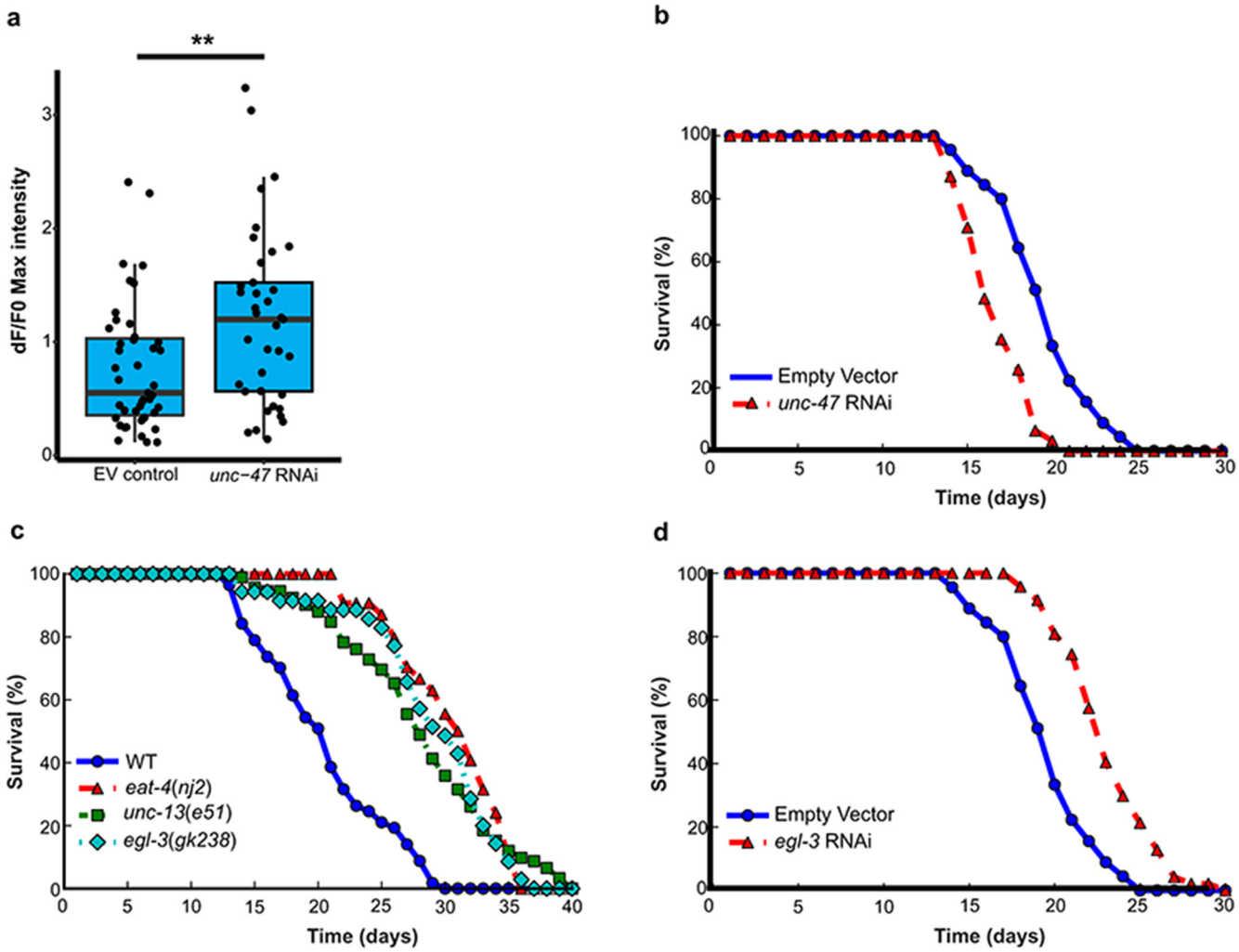

Extended Data Figure 4. Neural excitation, neuropeptide signaling and lifespan in *C. elegans*.

a, Increased excitation of ASH neurons following RNAi against the GABA vesicular transporter *unc-47*. GCaMP imaging was performed on worms with enhanced neuronal RNAi (See Figure 3 legend and Methods for details) for *unc-47* (n=37) or controls (n=43) at day 2. **P= 6.8e-3 by the Mann–Whitney U test. **b,** RNAi for *unc-47* reduces lifespan. Worms with enhanced neuronal RNAi were treated with *unc-47* (n=31) or control RNAi (n=84). Shown is a representative lifespan analysis replicated 3 times. P= 1.3e-6 by log-rank test. **c,** Reduction of synaptic neurotransmission or neuropeptide signaling extend lifespan in *C. elegans*. Mutations in genes affecting glutamatergic neurotransmission (*eat-4*), presynaptic function (*unc-13*) and neuropeptide signaling (*egl-3)* exhibit comparable lifespan extension. WT, n=57; *eat-4*(*nj2*), n=54. P≤2.2e-16; *unc-13*(*e51*), n=92, P=3.6e-14; *egl-3*(*gk238*), n=35, P=8.3e-11 by log-rank test. Shown are curves representative of two independent replicates. **d,** Extension of lifespan by *egl-3* RNAi in worms with enhanced neuronal RNAi. Shown are lifespan curves representative of two independent replicates. *egl-3* RNAi (n=47 worms); Empty Vector (n=84 worms). P=3.5e-11 by the log-rank test.

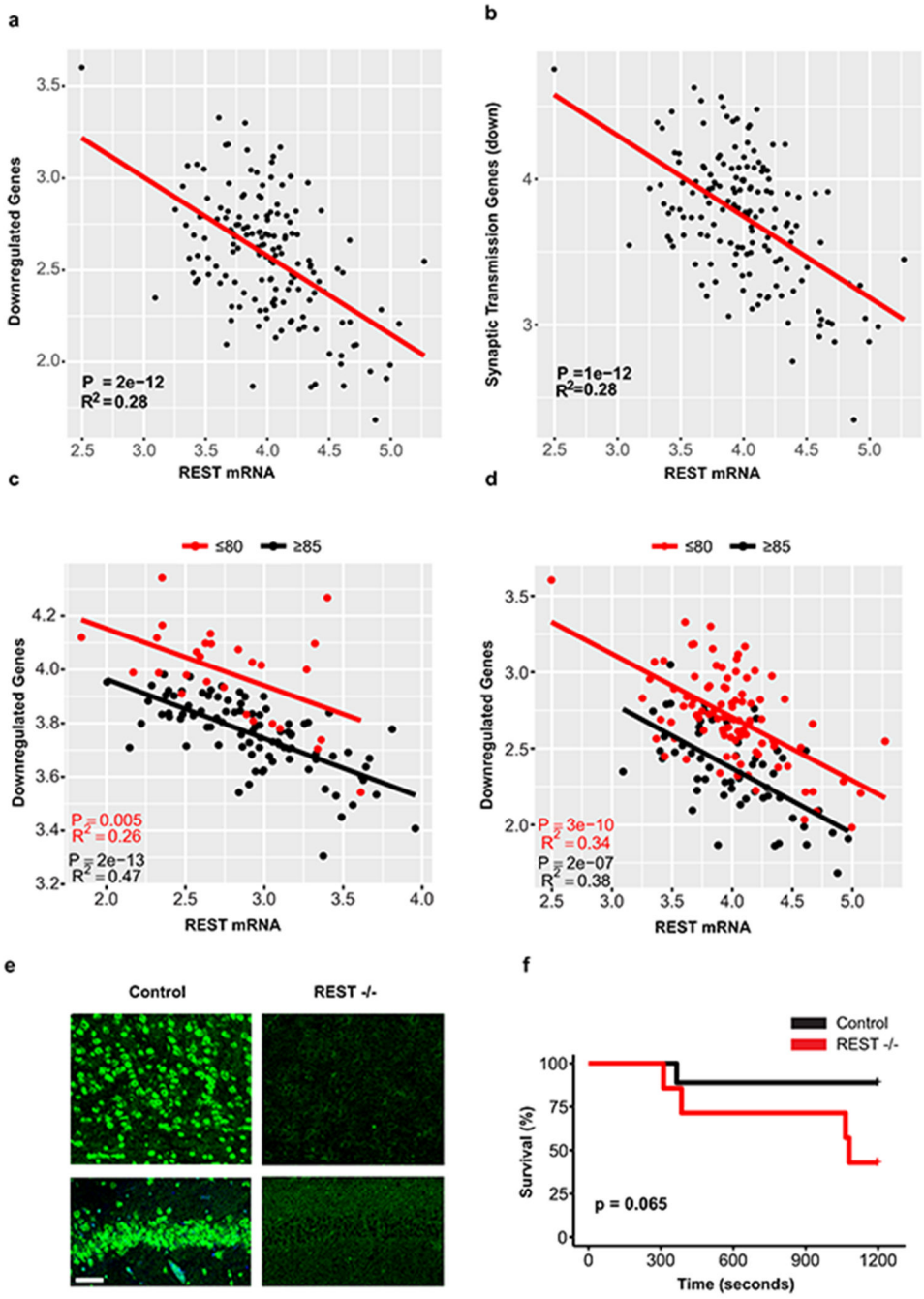

Extended Data Figure 5. Gene regulation and neural activity associated with REST and extended longevity.

a-b, Expression of genes downregulated in individuals ≥85 years versus ≤80 years old is inversely related to REST mRNA levels. Shown is linear regression analysis of normalized and adjusted REST mRNA levels and mean expression of **a,** all downregulated genes and **b,** downregulated genes associated with the synaptic transmission GO term. Data is from the CommonMind cohort. Each point represents an individual case, n=155 individuals. P-values were derived by a t-test for the slope of the regression line. Note similarity to the data for the

ROSMAP cohort in Fig. 2a, b. **c-d,** Stratification by age group. Analysis of the ROSMAP cohort (c, n=117 individuals) and the CommonMind cohort (d, n=155 individuals) as in Fig 2a, but stratified by age group. P-values were derived by t-test for the slope of the regression line. **e,** Loss of REST expression in conditional REST knockout mice. Representative images of the cortex (top panel) and hippocampus (bottom panel) from $REST^{lx/lx}$ (Control)**,** and Nestin-Cre;$REST^{lx/lx}$ (REST−/−) mice. Immunolabeling was performed with the anti-mouse REST-14 antibody directed against the REST C-terminal domain. Scale bar, 40 μm. Image shown is representative of an experiment replicated 4 times. **f,** Survival of REST −/− and control mice following administration of the seizure-inducing agent pentylentetrazole (PTZ, 40 mg/kg). P=0.065 for REST−/− versus control by the log-rank test. Control, n=9; REST−/−, n=7.

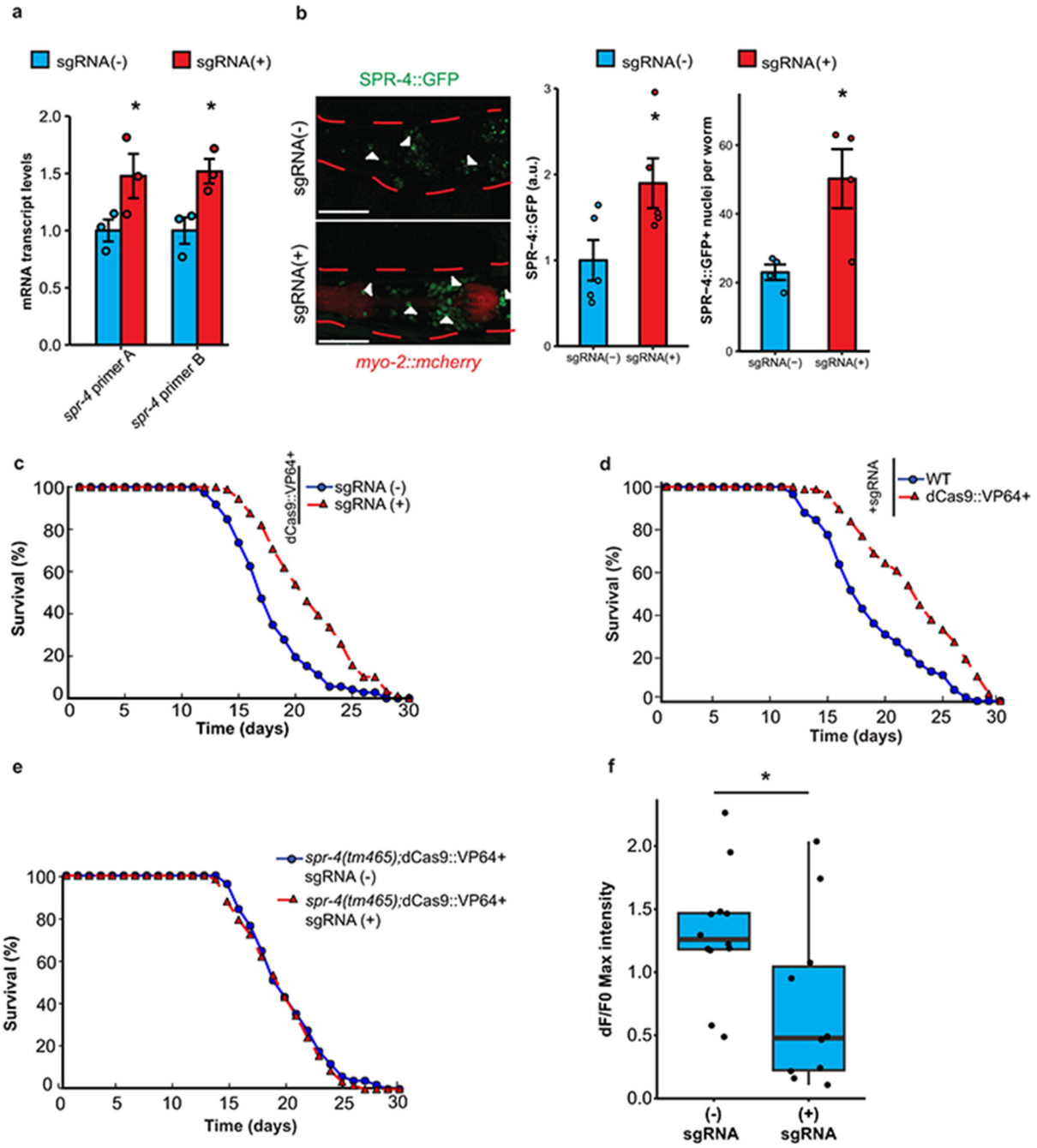

Extended Data Figure 6. Induction of *spr-4* extends lifespan and suppresses neural excitation in *C. elegans*.

a, *spr-4* mRNA levels in worms expressing a stably integrated dCas9::VP64 transgene in the presence, sgRNA(+), or absence sgRNA(−), of 4 different sgRNAs targeting the *spr-4* promoter. Transcript levels were determined by qRT-PCR and normalized to sgRNA(−) controls. Values are the mean ± S.E.M., n=3. A: *P= 0.041; B: P=0.020 by one-sided Student's *t*-test. **b,** dCas9::VP64-mediated elevation of SPR-4 protein levels. Left panel: Representative images of the head region of heterozygous F1 progeny of the strains bearing

a *pspr-4::spr-4::gfp::spr-4utr* transgene. Arrowheads indicate SPR-4::GFP positive nuclei. Dashed red lines indicate the outline of the worm body. Scale bar, 40 μm. Middle panel: Values represent the mean ± S.E.M. sgRNA(−), n=5 worms; sgRNA(+), n=5 worms with 7-38 measurements per worm; *P=0.022, one-sided Student's t-test. Right panel: Values represent the mean ± S.E.M. sgRNA(−), n=4 worms; sgRNA(+), n=4 worms. P=0.011, one-sided Student's t-test. Shown is a representative experiment replicated three times. **c,** Extended lifespan in worms expressing an integrated dCas9::VP64 transgene and sgRNAs targeting the *spr-4* promoter [sgRNA(+)] (n=79 worms) relative to dCas9::VP64-expressing worms in the absence of sgRNAs [sgRNA (−)] (n=57 worms) P=5.5e-9, log-rank test. Representative of an experiment replicated 6 times. **d**, Lifespans of worms expressing sgRNA targeting the *spr-4* promoter in the presence (n=87 worms) or absence (n=58 worms) of dCas9::VP64. P=3.7e-7, log-rank test. Representative of an experiment replicated twice. **e,** Lifespans of dCas9::VP64 expressing worms in the presence (n=51 worms) or absence (n=58 worms) of sgRNAs on the *spr-4(tm465)* loss-of-function mutant background. P=0.49, log-rank test. Representative of three independent replicates. **f,** Overexpression of *spr-4* reduces neural excitation. GCaMP imaging was performed in ASH neurons in SPR-4 overexpressing (sgRNA+) and control (sgRNA-) worms in the lines described in **c**. Shown are maximum GCaMP fluorescence changes. sgRNA minus, n=12 worms; sgRNA plus, n=10 worms. *P=0.025, Mann–Whitney U test.

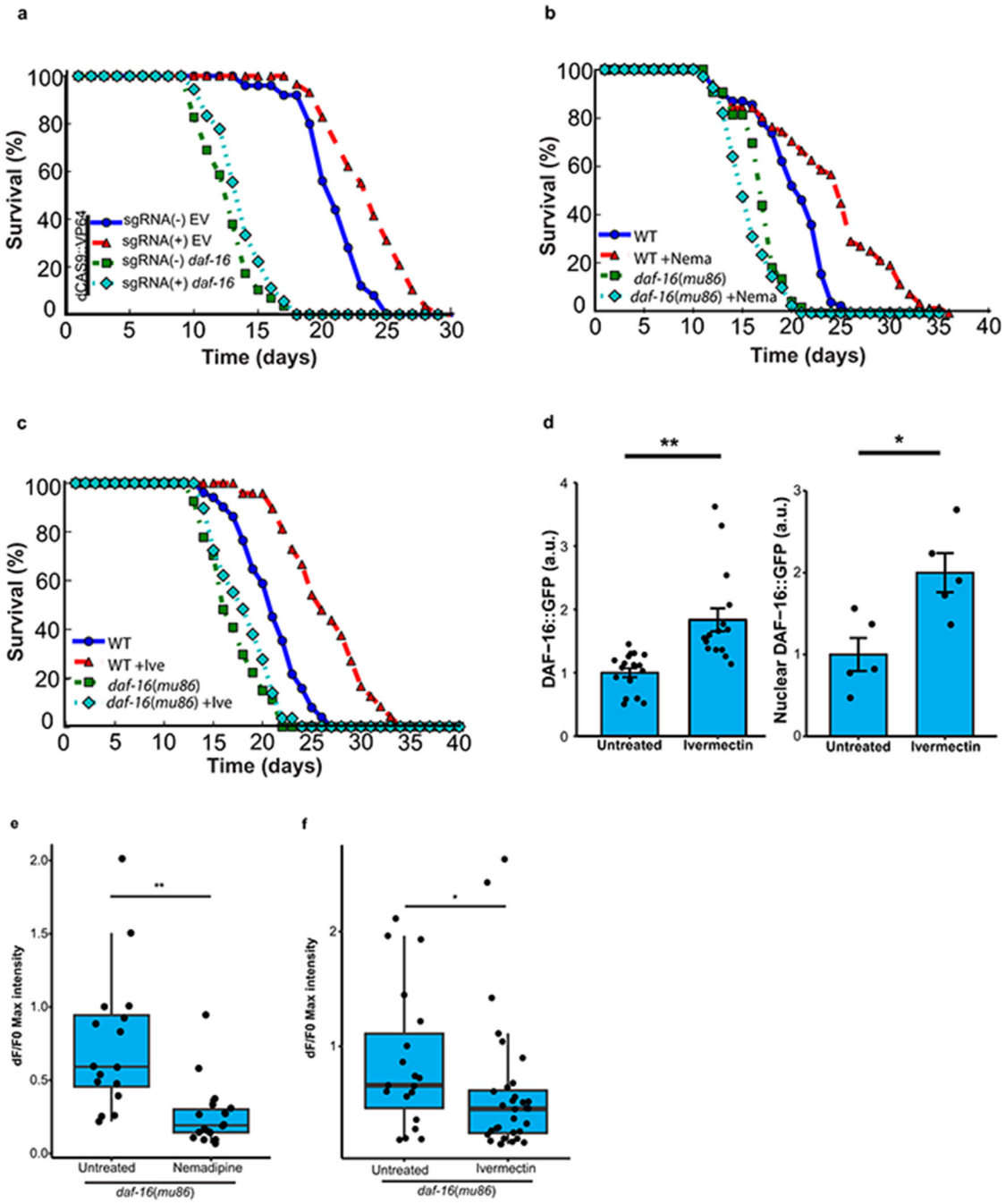

Extended Data Figure 7. Lifespan extension by *spr-4* overexpression and inhibition of neural excitation are *daf-16*-dependent.

a, Lifespan extension by overexpression of *spr-4* is *daf-16* dependent. Lifespans of worms overexpressing *spr-4* (sgRNA+;dCAS9::VP64) or not overexpressing *spr*-4 (sgRNA-;dCAS9::VP64) following treatment with *daf-16* RNAi or an empty vector control. sgRNA(+)EV (n=29 worms) versus sgRNA(−)EV (n=25 worms): P=2.7e-4; sgRNA(+)*daf-16* (n=18 worms) versus sgRNA(−)*daf-16* (n=29 worms) P=0.20 by log-rank test. Representative of 4 independent replicates. **b, c,** Lifespan extension by the neural

excitation inhibitors ivermectin and nemadipine is *daf-16*-dependent. Shown are lifespan determinations for WT control and *daf-16*(*mu86*) mutant worms in the presence or absence of nemadipine (2μM) (**b**) or ivermectin (1pg/ml) (**c**). **b,**WT, n=69 worms; WT+Nema, n=51; *daf-16*, n=43; *daf-16*+Nema, n=67. WT+Nema vs WT, P=9.9e-8; daf-16+Nema vs daf-16, P=0.014 by log-rank test **c,** WT, n=78 worms; WT+Ive, n=77; *daf-16*, n=27; *daf-16*+Ive, n=29. WT+Ive vs WT, P=7.3e-8; *daf-16*+Ive vs *daf-16*, P=0.22; log-rank test. Curves are representative of an experiment replicated 2 (nemadipine) or 3 (ivermectin) times. **d,** Inhibition of neural excitation with ivermectin elevates DAF-16 levels. Worms expressing a DAF-16::GFP transgene were treated for 10 days with 1 pg/mL ivermectin and assessed by confocal microscopy. Left panel: Shown is total DAF-16::GFP. Values represent the mean ± S.E.M (untreated, n=19 worms, Ivermectin, n=16 worms). **P=2.5e-7, Mann-Whitney U test. Right panel: Shown is nuclear DAF-16::GFP (n=5 worms per group, 50-61 nuclei per worm). *P= 0.013 by Student's t-test. Results are representative of an experiment replicated twice. **e,** DAF-16 is not required for inhibition of neural excitation by nemadipine. Shown are maximum ASH GCaMP intensity changes for day 2 *daf-16*(*mu86*) mutant worms treated for 24 hours with 2 μM nemadipine (untreated, n=16 worms; nemadipine, n=18 worms). P=9.4e-5, Mann-Whitney U test). **f,** DAF-16 is not required for inhibition of neural excitation by ivermectin. Shown are day 2 worms treated for 24 hours with 1 pg/mL ivermectin (control, n=19 worms; ivermectin, n=32 worms). P=0.030, Mann-Whitney U test).

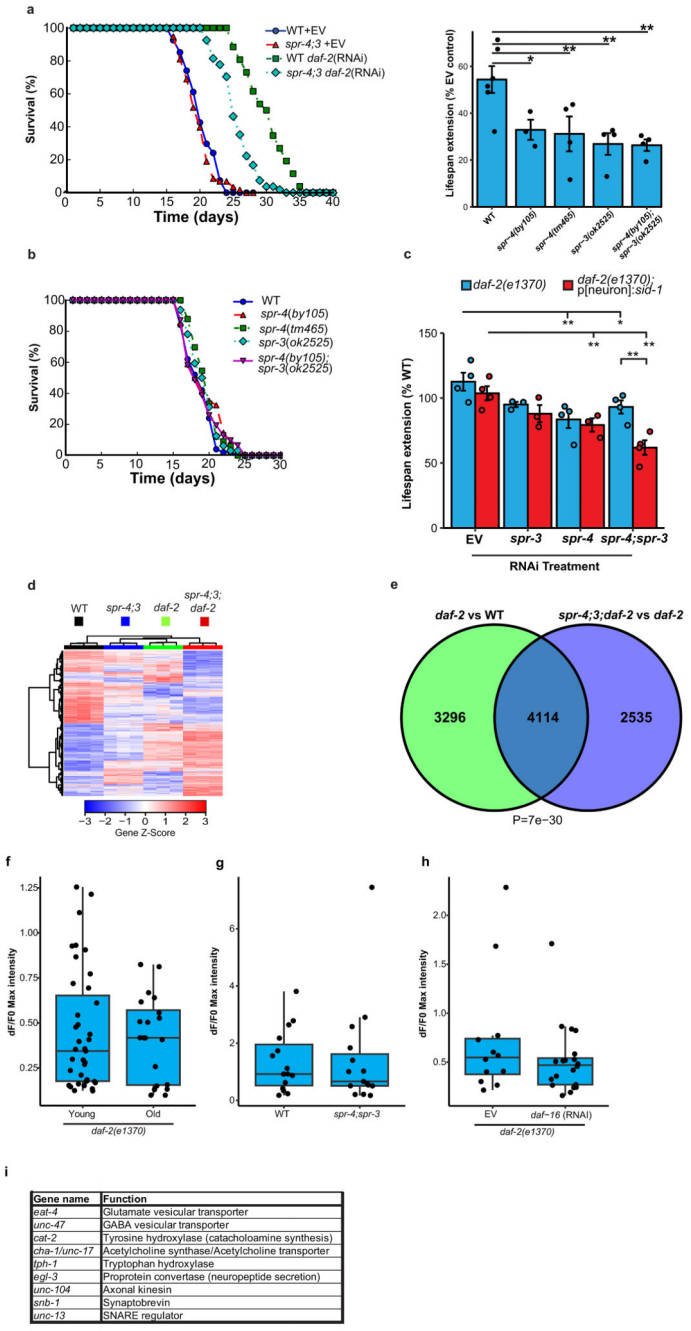

Gene name	Function
eat-4	Glutamate vesicular transporter
unc-47	GABA vesicular transporter
cat-2	Tyrosine hydroxylase (catacholoamine synthesis)
cha-1/unc-17	Acetylcholine synthase/Acetylcholine transporter
tph-1	Tryptophan hydroxylase
egl-3	Proprotein convertase (neuropeptide secretion)
unc-104	Axonal kinesin
snb-1	Synaptobrevin
unc-13	SNARE regulator

Extended Data Figure 8. SPR-3 and SPR-4 contribute to lifespan extension and gene regulation associated with reduced DAF-2 insulin/IGF-like signaling.

a, Loss of function of SPR-3 and SPR-4 reduces the lifespan extension of *daf-2* RNAi. Left panel: Representative lifespan analysis of *spr-4(by105);spr-3(ok2525)* double mutant and wild-type (WT) worms following *daf-2* or empty vector (EV) control RNAi. WT+EV, n=54 worms; *spr-4;3*+EV, n=58 worms; WT+*daf-2*, n=26 worms; *spr-4;3*+*daf-2*, n=54 worms. Right panel: Values represent mean percent lifespan extension ± S.E.M. (*daf-2* RNAi versus EV control) in the indicated genotypes. WT, n=6 independent experiments; *spr-4*(*by105*), n=3, *P=0.017 versus WT; *spr-4*(*tm465*), n=4, **P=0.0062 versus WT; *spr-3*(*ok2525*), n=4,

P=0.0018 versus WT; *spr-4*(*by105*);*spr-3*(*ok2525*), n=4, **P=0.0016 versus WT by Students *t*-test. See Supplementary Table 22 for individual lifespan data and statistics. **b, Lifespan is unaffected by *spr-4* and *spr-3* mutations in a wild-type background. WT, n=50 worms; *spr-3*(*ok2525*), n=31; *spr-4*(*by105*);*spr-3*(*ok2525*), n=32; *spr-4*(*by105*), n=34; *spr-4*(*tm465*), n=33.There were no reproducibly significant changes by the log-rank test in 3-6 independent experiments per genotype (see Supplementary Table 22). **c,** Quantification of lifespan extension in *daf-2* mutant worms shown in Fig. 3b attributable to neuronal expression of *spr-3* and *spr*-4. RNAi was targeted to neurons by neuronal expression of a *sid*-1 transgene in otherwise *sid-1* null *daf-2(1370)* mutants (*daf-2*;p[neuron]:*sid-1*), and compared with untargeted RNAi in *sid-1* wild-type *daf-2(1370)* mutants (*daf-2*). Values represent mean lifespan extension relative to the control *sid-1*(*pk3321*);p[neuron]:*sid-1* worms treated with empty vector (EV) ± S.E.M (n= 3 independent experiments). Significant lifespan effects were not observed for RNAi in the absence of the *daf-2* mutation. *P<0.05; **P<0.01 by Student's *t*-test. **d,** Gene expression determined by RNA sequencing in day 2 adult worms. Differentially expressed genes (rows) and the indicated worm genotypes (columns) were clustered, and gene expression, transformed to a z-score per gene, is represented in a heat map. N=3 independent replicates per genotype. **e**, Venn diagram illustrating the overlap of differentially expressed genes in *daf-2* single mutant vs WT and *spr-4;3;daf-2* triple mutant vs *daf-2* single mutant comparisons. P=7e-30, Fisher's exact test with a one-sided alternative hypothesis. **. f,** Long-lived *daf-2* mutants do not show an age-related increase in neural excitation. Shown is maximum ASH GCaMP intensity changes in day1-2 (n=39) and day 14-16 (n=20) *daf-2(e1370)* mutant worms. Note the absence of the age-related increase in excitation observed in wild-type aging worms (Fig. 1e). P=0.93, Mann-Whitney U test. **g**, The *spr-4;spr-3* double mutant in a wild-type background does not significantly affect neural excitation in ASH neurons. WT, n=15 worms; *spr-4;spr-3*, n=15 worms. P= 0.62, Mann-Whitney U test. **h,** DAF-16 does not mediate suppression of neural excitation in the *daf-2* mutant. RNAi for *daf-16* was performed in *daf-2(e1370)* mutant worms on a *sid-1*(*pk3321*);p[neuron]:*sid-1* background to augment RNAi in neurons (*daf-16* RNAi, n=20 worms, empty vector (EV) control, n=12 worms). P=0.33, Mann–Whitney U test. **i,** Description of the genes targeted by RNAi in Figure 4d.

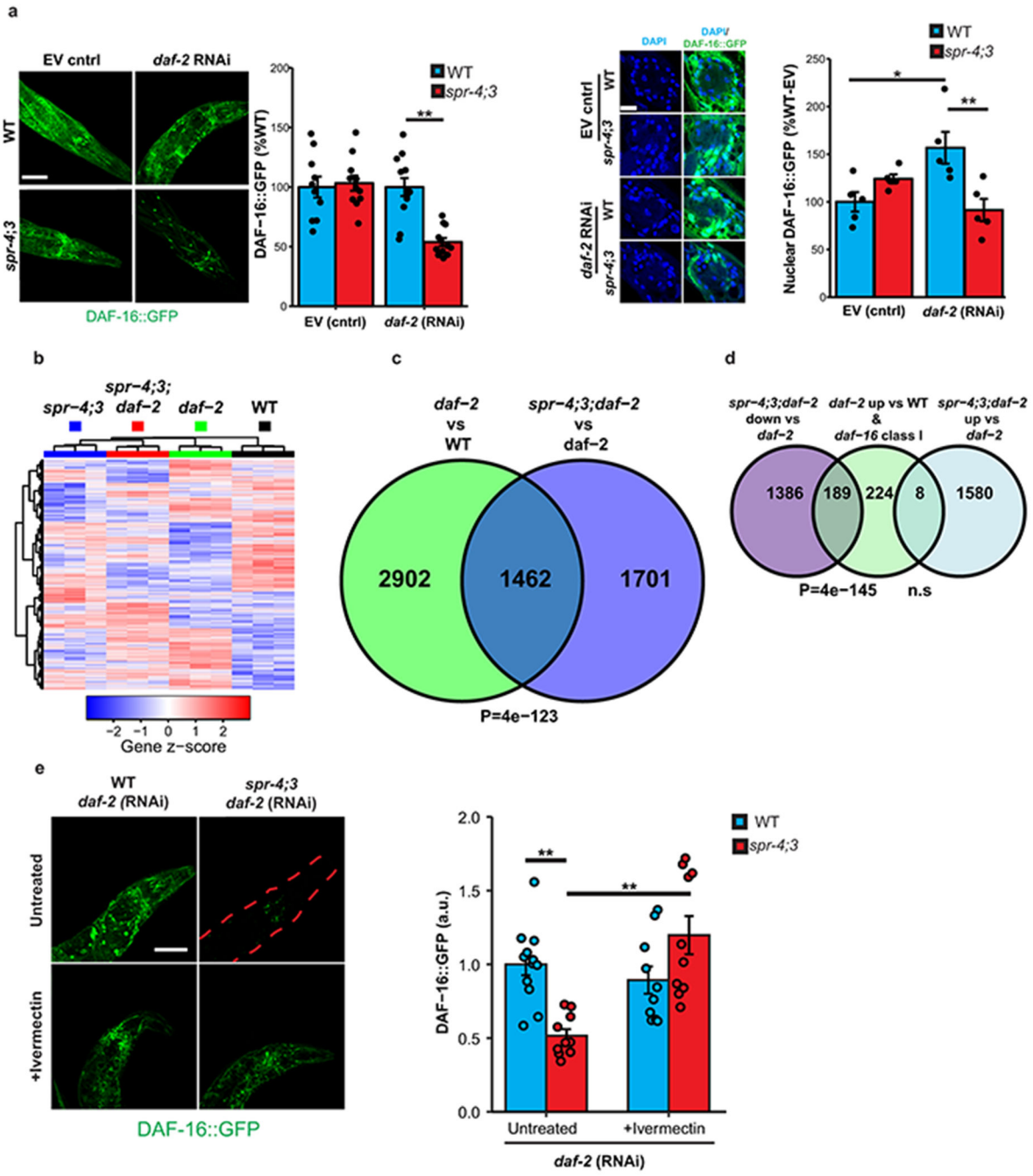

Extended Data Figure 9. Regulation of DAF-16 by SPR-3 and SPR-4.

a, Reduced DAF-16 activation in *spr-4;3* mutants following *daf-2* RNAi. Left confocal panel: Shown are day 10 worms of the indicated genotypes expressing an integrated DAF-16::GFP transgene and treated with *daf-2* RNAi or empty vector (EV) control since day 1 of adulthood. Images are maximum intensity z-projections. Scale bar, 40μm. Left bar graph: Values represent mean GFP intensity ± S.E.M. in the peri-pharyngeal regions of *spr-4;3* double mutants relative to wild-type controls for a representative experiment replicated 4 times (see methods for details of analysis). (n=8-12 worms per replicate).

P=5.2e-5 by Welch's t-test. Right confocal panel: Higher magnification views of DAF-16::GFP and DAPI-labeled nuclei. Images are magnified confocal z-planes. Scale bar, 10μm. Right bar graph: Values represent mean nuclear GFP intensity ± S.E.M. relative to the WT-EV control, n=5 worms per genotype and 51-89 nuclei per worm. *P=0.016, **P=5.5e-3 by ANOVA with post-hoc Tukey test. Values and images are representative of an experiment replicated 3 times. **b, Gene expression determined by RNA sequencing in adult day 10 worms. Differentially expressed genes (rows) and replicates of the indicated worm genotypes (columns) were clustered, and gene expression, transformed to a z-score per gene, is represented in a heat map. n=3 independent replicates per genotype. **c**, Venn diagram illustrating the overlap of differentially expressed genes in day 10 *daf-2* vs WT and *spr-4;3;daf-2* vs *daf-2* comparisons. P=4e-123, Fisher's exact test with a one-sided alternative hypothesis. **d,** Overlap of class I *daf-16* target genes (described in Methods) with genes downregulated in day 10 *spr-4;3;daf-2* triple mutants relative to *daf-2* single mutants. P-values were calculated using a hypergeometric distribution (see Methods). n.s, p=0.99 **e,** Ivermectin increases DAF-16::GFP levels in *spr-4;3* worms following *daf-2* RNAi. Left panel: Confocal imaging of GFP fluorescence in ivermectin-treated (10 pg/ml) and untreated worms. The red dashed lines indicate the worm body. Right panel: Quantification of DAF-16::GFP. Values represent mean GFP intensity ± S.E.M., WT/Untreated, n=12; WT/Ivermectin, n=10; *spr-4;*3/Untreated, n=10; *spr-4;*3/Ivermectin, n=10. **P=4.6e-4 (*spr-4;3* vs WT untreated), P=2.6e-4 (*spr-4;3* +Ivermectin vs *spr-4;3* untreated) by Mann–Whitney U test with multiple testing correction by Holm's method. Shown is a representative experiment replicated 3 times.

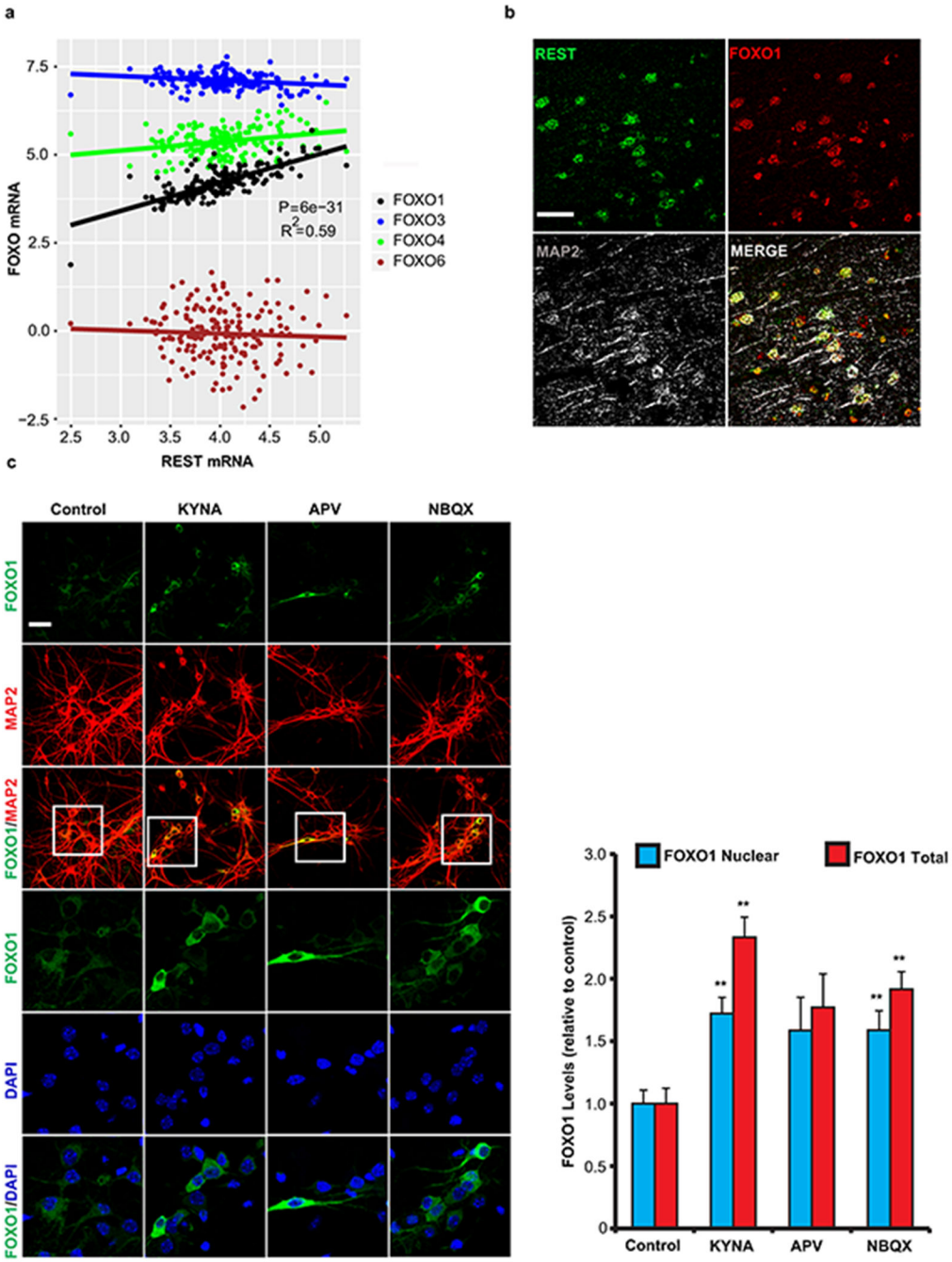

Extended Data Figure 10. Coregulation of FOXO1 and REST in the aging brain and modulation by glutamatergic signaling.

a, Linear regression analysis of REST and FOXO mRNA levels in the prefrontal cortex of 174 cognitively-intact individuals (age≥60 years) from the CommonMind Consortium determined by RNA sequencing. P-values are derived from a *t*-test for the slope of the regression line and Bonferroni-corrected across all expressed genes. **b,** Colocalization of REST and FOXO1 in neurons of the aged human prefrontal cortex. Confocal immunofluorescence microscopy was performed in human prefrontal cortex using

antibodies against REST (green, rabbit polyclonal; Bethyl), FOXO1 (red, goat polyclonal; LS-Bio) and the neuronal marker MAP2 (grey, chicken polyclonal; Abcam). Scale bar, 40 μm. The image shown is representative of immunofluorescence labeling performed in 30 individuals. See Supplementary Table 20 for additional information on antibodies. **c,** Inhibition of glutamatergic signaling in mouse cortical neuronal cultures elevates FOXO1 levels. Left panel: Primary mouse cortical neuronal cultures treated with kynurenic acid (KYNA, 5 μM), APV (50 μM), NBQX (2 μM) or vehicle (Control) were analyzed by confocal immunofluorescence for FOXO1 or MAP2 and labeled with DAPI. Boxed areas were magnified in the lower three rows. Note that most FOXO1 in cultured neurons is cytoplasmic, but a detectable nuclear component overlaps with DAPI. Scale bar, 40 μm. Right panel: Quantification of total and nuclear FOXO1 levels in MAP2-positive neurons. Values represent the mean ± S.E.M. Control, n=200; KYNA, n=326; APV, n=148; NBQX, n=197. FOXO1 Total/KYNA: **P=2.1e-8; FOXO1 Nuclear/KYNA **P=1.1e-4; FOXO1 Total/NBQX **P=8.8e-13; FOXO1 nuclear/NBQX **P=5.2e-6 by the Mann–Whitney U test with multiple testing correction by Holm's method. Shown is a representative experiment replicated 3 times.

Supplementary Material

Refer to Web version on PubMed Central for supplementary material.

Acknowledgements:

We thank members of the Yankner laboratory for suggestions and discussion, and the Hsieh laboratory for providing the anti-mouse REST antibody. This work was supported by an NIH Director's Pioneer Award (DP1OD006849) and NIH grants RO1AG046174 and RO1AG26651 to B.A.Y., RO1GM072551 to M.P.C., P30AG10161, R01AG15819, R01AG17917, R01AG36836, U01AG46152 to D.A.B, EY024376 to C.-A.M., EY011930 to W.H.K., K99AG050830 to J.Z., and grants from the Glenn Foundation for Medical Research and The Ludwig Family Foundation to B.A.Y.

Data were generated as part of the CommonMind Consortium supported by funding from Takeda Pharmaceuticals Company Limited, F. Hoffman-La Roche Ltd and NIH grants R01MH085542, R01MH093725, P50MH066392, P50MH080405, R01MH097276, RO1-MH-075916, P50M096891, P50MH084053S1, R37MH057881 and R37MH057881S1, HHSN271201300031C, AG02219, AG05138 and MH06692.

References

1. Satoh A, Imai S-i, Guarente L. The brain, sirtuins, and ageing. Nat Rev Neurosci. 2017;18(6):362–74. [PubMed: 28515492]
2. Bishop NA, Lu T, Yankner BA. Neural mechanisms of ageing and cognitive decline. Nature. 2010;464(7288):529–35. [PubMed: 20336135]
3. Ailion M, Inoue T, Weaver CI, Holdcraft RW, Thomas JH. Neurosecretory control of aging in Caenorhabditis elegans. Proc Natl Acad Sci U S A. 1999;96(13):7394–7. [PubMed: 10377425]
4. Apfeld J, Kenyon C. Regulation of lifespan by sensory perception in Caenorhabditis elegans. Nature. 1999;402(6763):804–9. [PubMed: 10617200]
5. Alcedo J, Kenyon C. Regulation of C. elegans longevity by specific gustatory and olfactory neurons. Neuron. 2004;41(1):45–55. [PubMed: 14715134]
6. Bishop NA, Guarente L. Two neurons mediate diet-restriction-induced longevity in C. elegans. Nature. 2007;447(7144):545–9. [PubMed: 17538612]
7. Wolkow CA, Kimura KD, Lee M-S, Ruvkun G. Regulation of C. elegans Life-Span by Insulinlike Signaling in the Nervous System. Science. 2000;290(5489):147–50. [PubMed: 11021802]

8. Lu T, Pan Y, Kao SY, Li C, Kohane I, Chan J, Yankner BA. Gene regulation and DNA damage in the ageing human brain. Nature. 2004;429(6994):883–91. [PubMed: 15190254]
9. Mostafavi S, Gaiteri C, Sullivan SE, White CC, Tasaki S, Xu J, Taga M, Klein HU, Patrick E, Komashko V, McCabe C, Smith R, Bradshaw EM, Root DE, Regev A, Yu L, Chibnik LB, Schneider JA, Young-Pearse TL, Bennett DA, De Jager PL. A molecular network of the aging human brain provides insights into the pathology and cognitive decline of Alzheimer's disease. Nat Neurosci. 2018;21(6):811–9. [PubMed: 29802388]
10. Fromer M, Roussos P, Sieberts SK, Johnson JS, Kavanagh DH, Perumal TM, Ruderfer DM, Oh EC, Topol A, Shah HR, Klei LL, Kramer R, Pinto D, Gumus ZH, Cicek AE, Dang KK, Browne A, Lu C, Xie L, Readhead B, Stahl EA, Xiao J, Parvizi M, Hamamsy T, Fullard JF, Wang YC, Mahajan MC, Derry JM, Dudley JT, Hemby SE, Logsdon BA, Talbot K, Raj T, Bennett DA, De Jager PL, Zhu J, Zhang B, Sullivan PF, Chess A, Purcell SM, Shinobu LA, Mangravite LM, Toyoshiba H, Gur RE, Hahn CG, Lewis DA, Haroutunian V, Peters MA, Lipska BK, Buxbaum JD, Schadt EE, Hirai K, Roeder K, Brennand KJ, Katsanis N, Domenici E, Devlin B, Sklar P. Gene expression elucidates functional impact of polygenic risk for schizophrenia. Nat Neurosci. 2016;19(11):1442–53. [PubMed: 27668389]
11. Gibbs JR, van der Brug MP, Hernandez DG, Traynor BJ, Nalls MA, Lai SL, Arepalli S, Dillman A, Rafferty IP, Troncoso J, Johnson R, Zielke HR, Ferrucci L, Longo DL, Cookson MR, Singleton AB. Abundant quantitative trait loci exist for DNA methylation and gene expression in human brain. PLoS Genet. 2010;6(5):e1000952. [PubMed: 20485568]
12. Hilliard MA, Apicella AJ, Kerr R, Suzuki H, Bazzicalupo P, Schafer WR. In vivo imaging of C. elegans ASH neurons: cellular response and adaptation to chemical repellents. The EMBO Journal. 2005;24(1):63–72. [PubMed: 15577941]
13. Pokala N, Liu Q, Gordus A, Bargmann CI. Inducible and titratable silencing of Caenorhabditis elegans neurons in vivo with histamine-gated chloride channels. Proc Natl Acad Sci U S A. 2014;111(7):2770–5. [PubMed: 24550306]
14. Hamilton B, Dong Y, Shindo M, Liu W, Odell I, Ruvkun G, Lee SS. A systematic RNAi screen for longevity genes in C. elegans. Genes & Development. 2005;19(13):1544–55. [PubMed: 15998808]
15. Lu T, Aron L, Zullo J, Pan Y, Kim H, Chen Y, Yang T-H, Kim H-M, Drake D, Liu XS, Bennett DA, Colaiacovo MP, Yankner BA. REST and stress resistance in ageing and Alzheimer/'s disease. Nature. 2014;507(7493):448–54. [PubMed: 24670762]
16. Hu XL, Cheng X, Cai L, Tan GH, Xu L, Feng XY, Lu TJ, Xiong H, Fei J, Xiong ZQ. Conditional deletion of NRSF in forebrain neurons accelerates epileptogenesis in the kindling model. Cereb Cortex. 2011;21(9):2158–65. [PubMed: 21339379]
17. Brennan GP, Dey D, Chen Y, Patterson KP, Magnetta EJ, Hall AM, Dube CM, Mei YT, Baram TZ. Dual and Opposing Roles of MicroRNA-124 in Epilepsy Are Mediated through Inflammatory and NRSF-Dependent Gene Networks. Cell Rep. 2016;14(10):2402–12. [PubMed: 26947066]
18. Gilbert Luke A, Larson Matthew H, Morsut L, Liu Z, Brar Gloria A, Torres Sandra E, Stern-Ginossar N, Brandman O, Whitehead Evan H, Doudna Jennifer A, Lim Wendell A, Weissman Jonathan S, Qi Lei S. CRISPR-Mediated Modular RNA-Guided Regulation of Transcription in Eukaryotes. Cell. 2013;154(2):442–51. [PubMed: 23849981]
19. Lithgow GJ, White TM, Melov S, Johnson TE. Thermotolerance and extended life-span conferred by single-gene mutations and induced by thermal stress. Proc Natl Acad Sci U S A. 1995;92(16): 7540–4. [PubMed: 7638227]
20. Yang P, Sun R, Yao M, Chen W, Wang Z, Fei J. A C-terminal truncated mutation of spr-3 gene extends lifespan in Caenorhabditis elegans. Acta Biochim Biophys Sin (Shanghai). 2013;45(7): 540–8. [PubMed: 23692984]
21. Calixto A, Chelur D, Topalidou I, Chen X, Chalfie M. Enhanced neuronal RNAi in C. elegans using SID-1. Nat Methods. 2010;7(7):554–9. [PubMed: 20512143]
22. Lin K, Dorman JB, Rodan A, Kenyon C. daf-16: An HNF-3/forkhead family member that can function to double the life-span of Caenorhabditis elegans. Science. 1997;278(5341):1319–22. [PubMed: 9360933]
23. Evason K, Huang C, Yamben I, Covey DF, Kornfeld K. Anticonvulsant medications extend worm life-span. Science. 2005;307(5707):258–62. [PubMed: 15653505]

24. Evason K, Collins JJ, Huang C, Hughes S, Kornfeld K. Valproic acid extends Caenorhabditis elegans lifespan. Aging Cell. 2008;7(3):305–17. [PubMed: 18248662]
25. Chen X, McCue HV, Wong SQ, Kashyap SS, Kraemer BC, Barclay JW, Burgoyne RD, Morgan A. Ethosuximide ameliorates neurodegenerative disease phenotypes by modulating DAF-16/FOXO target gene expression. Mol Neurodegener. 2015;10:51. [PubMed: 26419537]
26. Pozzi D, Lignani G, Ferrea E, Contestabile A, Paonessa F, D'Alessandro R, Lippiello P, Boido D, Fassio A, Meldolesi J, Valtorta F, Benfenati F, Baldelli P. REST/NRSF-mediated intrinsic homeostasis protects neuronal networks from hyperexcitability. EMBO J. 2013;32(22):2994–3007. [PubMed: 24149584]
27. Pecoraro-Bisogni F, Lignani G, Contestabile A, Castroflorio E, Pozzi D, Rocchi A, Prestigio C, Orlando M, Valente P, Massacesi M, Benfenati F, Baldelli P. REST-Dependent Presynaptic Homeostasis Induced by Chronic Neuronal Hyperactivity. Mol Neurobiol. 2017.
28. Li Y, Wang WJ, Cao H, Lu J, Wu C, Hu FY, Guo J, Zhao L, Yang F, Zhang YX, Li W, Zheng GY, Cui H, Chen X, Zhu Z, He H, Dong B, Mo X, Zeng Y, Tian XL. Genetic association of FOXO1A and FOXO3A with longevity trait in Han Chinese populations. Hum Mol Genet. 2009;18(24): 4897–904. [PubMed: 19793722]
29. Bennett DA, Schneider JA, Arvanitakis Z, Wilson RS. Overview and findings from the religious orders study. Curr Alzheimer Res. 2012;9(6):628–45. [PubMed: 22471860]
30. Bennett DA, Schneider JA, Buchman AS, Barnes LL, Boyle PA, Wilson RS. Overview and findings from the rush Memory and Aging Project. Curr Alzheimer Res. 2012;9(6):646–63. [PubMed: 22471867]
31. Mu X, Fu X, Sun H, Beremand PD, Thomas TL, Klein WH. A gene network downstream of transcription factor Math5 regulates retinal progenitor cell competence and ganglion cell fate. Dev Biol. 2005;280(2):467–81. [PubMed: 15882586]
32. Mao CA, Tsai WW, Cho JH, Pan P, Barton MC, Klein WH. Neuronal transcriptional repressor REST suppresses an Atoh7-independent program for initiating retinal ganglion cell development. Dev Biol. 2011;349(1):90–9. [PubMed: 20969844]
33. Dhamne SC, Silverman JL, Super CE, Lammers SHT, Hameed MQ, Modi ME, Copping NA, Pride MC, Smith DG, Rotenberg A, Crawley JN, Sahin M. Replicable in vivo physiological and behavioral phenotypes of the Shank3B null mutant mouse model of autism. Mol Autism. 2017;8:26. [PubMed: 28638591]
34. Kelly E, Schaeffer SM, Dhamne SC, Lipton JO, Lindemann L, Honer M, Jaeschke G, Super CE, Lammers SH, Modi ME, Silverman JL, Dreier JR, Kwiatkowski DJ, Rotenberg A, Sahin M. mGluR5 Modulation of Behavioral and Epileptic Phenotypes in a Mouse Model of Tuberous Sclerosis Complex. Neuropsychopharmacology. 2018;43(6):1457–65. [PubMed: 29206810]
35. Purtell H, Dhamne SC, Gurnani S, Bainbridge E, Modi ME, Lammers SHT, Super CE, Hameed MQ, Johnson EL 3rd, Sahin M, Rotenberg A. Electrographic spikes are common in wildtype mice. Epilepsy Behav. 2018;89:94–8. [PubMed: 30399547]
36. Yuskaitis CJ, Jones BM, Wolfson RL, Super CE, Dhamne SC, Rotenberg A, Sabatini DM, Sahin M, Poduri A. A mouse model of DEPDC5-related epilepsy: Neuronal loss of Depdc5 causes dysplastic and ectopic neurons, increased mTOR signaling, and seizure susceptibility. Neurobiol Dis. 2018;111:91–101. [PubMed: 29274432]
37. Brenner S The genetics of Caenorhabditis elegans. Genetics. 1974;77(1):71–94. [PubMed: 4366476]
38. Lakowski B, Eimer S, Göbel C, Böttcher A, Wagler B, Baumeister R. Two suppressors of sel-12 encode C2H2 zinc-finger proteins that regulate presenilin transcription in Caenorhabditis elegans. Development. 2003;130(10):2117–28. [PubMed: 12668626]
39. Kenyon C, Chang J, Gensch E, Rudner A, Tabtiang R. A C. elegans mutant that lives twice as long as wild type. Nature. 1993;366(6454):461–4. [PubMed: 8247153]
40. Ohnishi N, Kuhara A, Nakamura F, Okochi Y, Mori I. Bidirectional regulation of thermotaxis by glutamate transmissions in Caenorhabditis elegans. The EMBO Journal. 2011;30(7):1376–88. [PubMed: 21304490]

41. Jarriault S, Greenwald I. Suppressors of the egg-laying defective phenotype of sel-12 presenilin mutants implicate the CoREST corepressor complex in LIN-12/Notch signaling in C. elegans. Genes & Development. 2002;16(20):2713–28. [PubMed: 12381669]
42. Winston WM, Molodowitch C, Hunter CP. Systemic RNAi in C. elegans requires the putative transmembrane protein SID-1. Science. 2002;295(5564):2456–9. [PubMed: 11834782]
43. Consortium CeDM. large-scale screening for targeted knockouts in the Caenorhabditis elegans genome. G3 (Bethesda). 2012;2(11):1415–25. [PubMed: 23173093]
44. Nottke AC, Beese-Sims SE, Pantalena LF, Reinke V, Shi Y, Colaiacovo MP. SPR-5 is a histone H3K4 demethylase with a role in meiotic double-strand break repair. Proc Natl Acad Sci U S A. 2011;108(31):12805–10. [PubMed: 21768382]
45. Greer EL, Becker B, Latza C, Antebi A, Shi Y. Mutation of C. elegans demethylase spr-5 extends transgenerational longevity. Cell Res. 2016;26(2):229–38. [PubMed: 26691751]
46. Robert VJ, Katic I, Bessereau JL. Mos1 transposition as a tool to engineer the Caenorhabditis elegans genome by homologous recombination. Methods. 2009;49(3):263–9. [PubMed: 19250968]
47. Kamath RS, Ahringer J. Genome-wide RNAi screening in Caenorhabditis elegans. Methods. 2003;30(4):313–21. [PubMed: 12828945]
48. Frokjaer-Jensen C, Davis MW, Ailion M, Jorgensen EM. Improved Mos1-mediated transgenesis in C. elegans. Nat Methods. 2012;9(2):117–8. [PubMed: 22290181]
49. Sarov M, Murray JI, Schanze K, Pozniakovski A, Niu W, Angermann K, Hasse S, Rupprecht M, Vinis E, Tinney M, Preston E, Zinke A, Enst S, Teichgraber T, Janette J, Reis K, Janosch S, Schloissnig S, Ejsmont RK, Slightam C, Xu X, Kim SK, Reinke V, Stewart AF, Snyder M, Waterston RH, Hyman AA. A genome-scale resource for in vivo tag-based protein function exploration in C. elegans. Cell. 2012;150(4):855–66. [PubMed: 22901814]
50. Dobin A, Davis CA, Schlesinger F, Drenkow J, Zaleski C, Jha S, Batut P, Chaisson M, Gingeras TR. STAR: ultrafast universal RNA-seq aligner. Bioinformatics. 2013;29(1):15–21. [PubMed: 23104886]
51. Liao Y, Smyth GK, Shi W. featureCounts: an efficient general purpose program for assigning sequence reads to genomic features. Bioinformatics. 2014;30(7):923–30. [PubMed: 24227677]
52. Robinson MD, McCarthy DJ, Smyth GK. edgeR: a Bioconductor package for differential expression analysis of digital gene expression data. Bioinformatics. 2010;26(1):139–40. [PubMed: 19910308]
53. Benjamini Y, Hochberg Y. Controlling the False Discovery Rate: A Practical and Powerful Approach to Multiple Testing. Journal of the Royal Statistical Society Series B (Methodological). 1995;57(1):289–300.
54. Sandelin A, Alkema W, Engstrom P, Wasserman WW, Lenhard B. JASPAR: an open-access database for eukaryotic transcription factor binding profiles. Nucleic Acids Res. 2004;32(Database issue):D91–4. [PubMed: 14681366]
55. Grant CE, Bailey TL, Noble WS. FIMO: scanning for occurrences of a given motif. Bioinformatics. 2011;27(7):1017–8. [PubMed: 21330290]
56. Chen EY, Tan CM, Kou Y, Duan Q, Wang Z, Meirelles GV, Clark NR, Ma'ayan A. Enrichr: interactive and collaborative HTML5 gene list enrichment analysis tool. BMC Bioinformatics. 2013;14:128. [PubMed: 23586463]
57. Zhang Y, Chen K, Sloan SA, Bennett ML, Scholze AR, O'Keeffe S, Phatnani HP, Guarnieri P, Caneda C, Ruderisch N, Deng S, Liddelow SA, Zhang C, Daneman R, Maniatis T, Barres BA, Wu JQ. An RNA-sequencing transcriptome and splicing database of glia, neurons, and vascular cells of the cerebral cortex. J Neurosci. 2014;34(36):11929–47. [PubMed: 25186741]
58. Tepper RG, Ashraf J, Kaletsky R, Kleemann G, Murphy CT, Bussemaker HJ. PQM-1 complements DAF-16 as a key transcriptional regulator of DAF-2-mediated development and longevity. Cell. 2013;154(3):676–90. [PubMed: 23911329]
59. Alexa A RJ. topGO: Enrichment Analysis for Gene Ontology R package version 2340 (2018).
60. Wang M, Zhao Y, Zhang B. Efficient Test and Visualization of Multi-Set Intersections. Sci Rep. 2015;5:16923. [PubMed: 26603754]

61. LIptak T On the Combination of independent tests. Magyar Tud Akad Mat Kutato Int Kozl. 1958(3):171–97.

62. Dewey M Metap: Meta Analysis of Significance Values R package Version 10. 2018.

63. Zaykin DV. Optimally weighted Z-test is a powerful method for combining probabilities in meta-analysis. J Evol Biol. 2011;24(8):1836–41. [PubMed: 21605215]

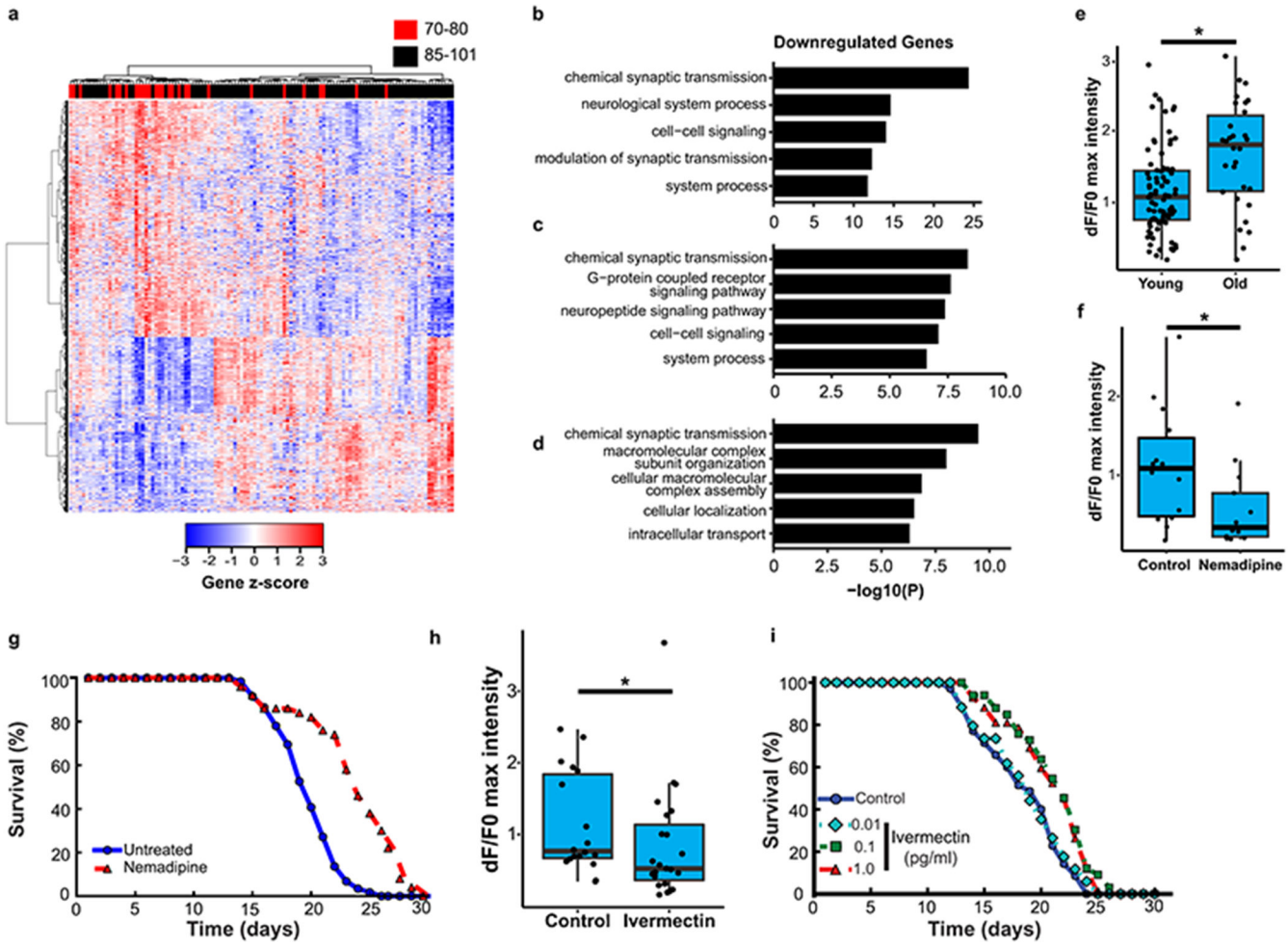

Figure 1.

Neural excitation and longevity in humans and *C. elegans*. **a,** Analysis of the cortical transcriptome profile in cognitively intact aged individuals from the ROSMAP cohort. Unsupervised hierarchical clustering shows a transcriptional signature of down- and up-regulated genes associated with extended longevity. **b-d**, Most significantly enriched gene ontology (GO) terms for downregulated genes associated with extended longevity (≥85 versus ≤80 years of age) in the ROSMAP (dorsolateral prefrontal cortex, n=117) (b), CommonMind Consortium (dorsolateral prefrontal cortex, n=155) (c), and Gibbs (frontal cortex, n=37) (d) cohorts. P-values were calculated by Fisher's exact test (see Methods). **e,** Aging *C. elegans* exhibit increased neuronal excitation. Shown are the maximum GCaMP fluorescence intensity changes in ASH neurons of young adult (day 1-2) and older (day 12-16) worms. Young, n=82 worms; Old, n=30 worms. *P=3.6e-4 by Mann–Whitney U test. **f,** The L-type calcium channel blocker nemadipine (2μM) represses neural excitation. Control, n=14; Nemadipine, n=13. *P=0.029, Mann–Whitney U test. **g**, Nemadipine extends lifespan. Worms were continuously treated with 2 μM nemadipine beginning at adult day 1, P=7.7e-11, log-rank test. Control, n=59; Nemadipine, n=50, replicated 3 times. **h,** The chloride channel agonist ivermectin (1pg/ml) reduces neural excitation. Control, n=18; Ivermectin, n=23. *P=0.038, Mann–Whitney U test. **i,** Extension of lifespan by continuous

treatment with ivermectin beginning at adult day 1 (Control, n=35; 0.01 pg/ml: n=34, P= 0.62 ; 0.1 pg/ml: n=33, P= 1.5e-3; 1pg/ml: n=42, P= 1.9e-3, log-rank test), replicated 3 times. Summary statistics for all individual lifespan experiments are in Supplementary Table 22.

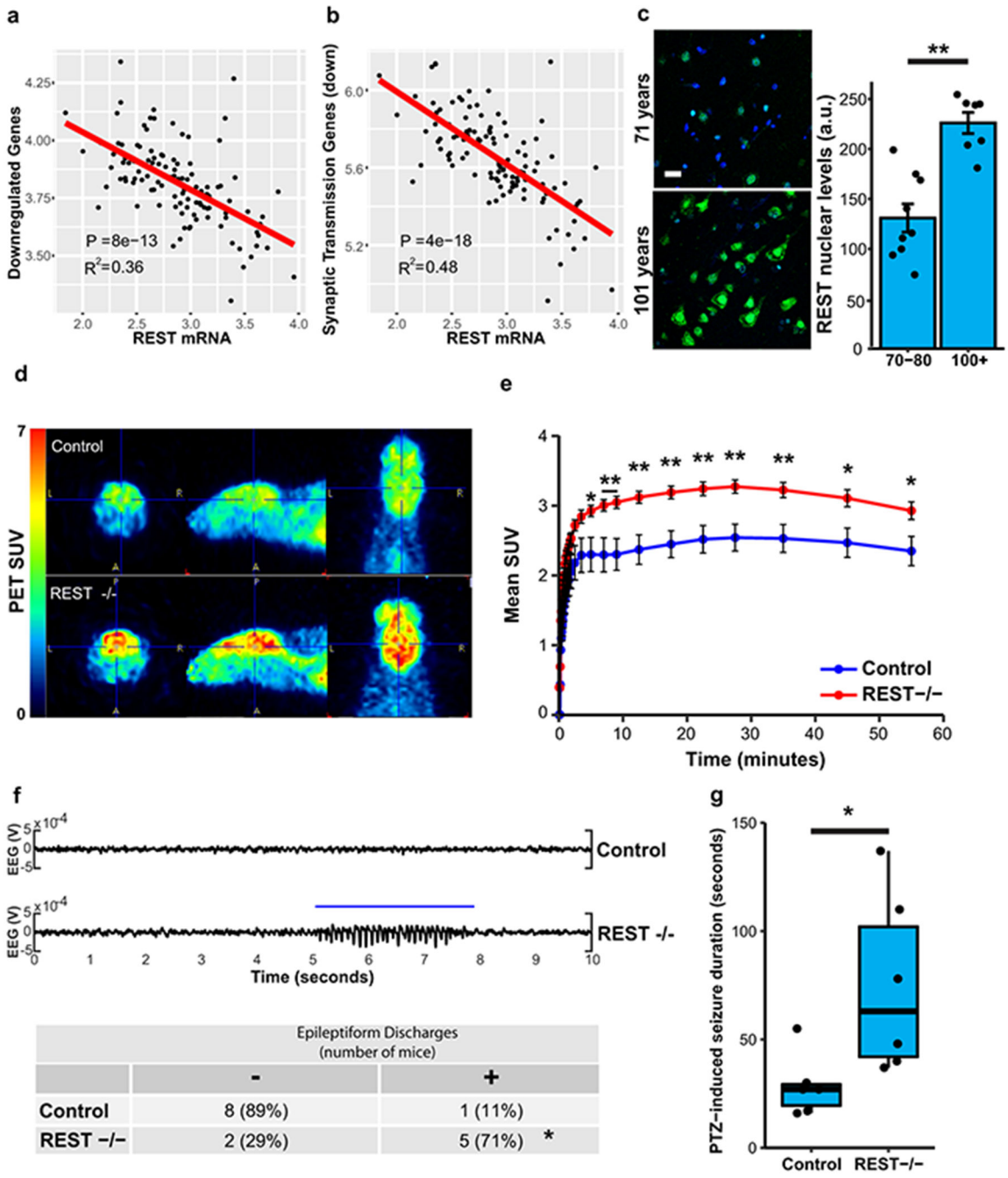

	Epileptiform Discharges (number of mice)	
	-	+
Control	8 (89%)	1 (11%)
REST −/−	2 (29%)	5 (71%) *

Figure 2.

REST regulates neural excitation in the aging brain and is associated with extended longevity. **a-b,** Expression of genes downregulated in individuals with extended longevity (≥85 versus ≤80 years old) is inversely related to REST mRNA levels. Shown is linear regression analysis of the mean expression of **a,** all downregulated genes and **b,** downregulated genes associated with the synaptic transmission GO term. Data is from the ROSMAP cohort. Each point represents an individual case (n=117). P-values were derived by t-tests of the regression line slopes. **c,** Increased nuclear REST levels in the prefrontal

cortex of centenarians. Left panel: Immunofluorescence labeling for REST (green, rabbit polyclonal; Bethyl laboratories) and DAPI (blue) in human prefrontal cortex. Scale bar, 40 μm. Right panel: Nuclear REST levels in cognitively intact individuals 70-80 years (n=9) and >100 years (n=7) of age. Values represent the mean ± S.E.M, **P=1.5e-4, Student's *t*-test. **d,** REST represses neural excitation in the mouse cerebral cortex. Shown are images from PET-CT scanning of fluorodeoxyglucose (^{18}F-FDG) uptake in 18-month-old Nestin-Cre;REST$^{lx/lx}$ (REST−/−) and age-matched REST$^{lx/lx}$ (Control) mice. **e,** Average standardized uptake value (SUV) at increasing time intervals after injection of ^{18}F-FDG. Values represent the mean ± S.E.M., n=7 mice per group. *P<0.05, **P<0.01, Mann-Whitney U test. **f,** Increased epileptiform discharges in aged REST-deficient mice. Upper Panel: EEG recording from REST(−/−) and age-matched control mice. Lower Panel: Number of mice with at least one epileptiform discharge (≥ 3 secs) in a 48 hour recording. Control, n=9; REST−/−, n=7. *P=0.035, Fisher's exact test. **g,** Seizure duration after administration of PTZ (40 mg/kg). Control, n=6; REST −/−, n=6 mice. *P=0.016, Mann–Whitney U test.

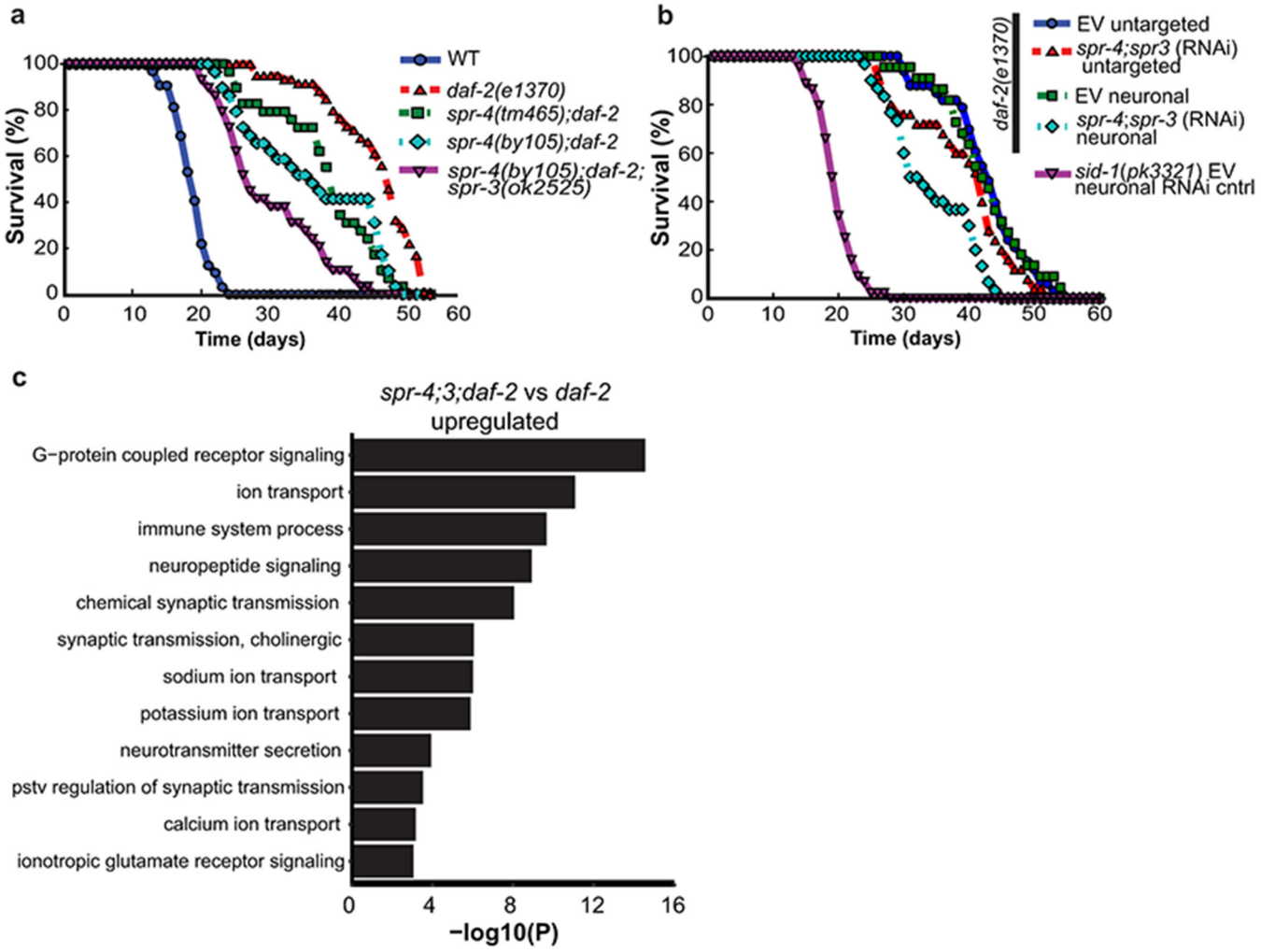

Figure 3.

C. elegans REST orthologs mediate longevity in *daf*-2 loss-of-function mutants. **a,** The REST orthologs s*pr-4* and *spr-3* are required for maximal longevity in *daf-2* mutant worms. Lifespan analysis was performed on wild-type and *daf-2(1370)* loss-of-function mutant worms, and the indicated combinations of *daf-2* and *spr-4/spr-3* mutations. The *spr-4/spr-3* mutations significantly reduced the lifespan of *daf-2* mutant worms. n=29-59 worms per genotype, replicated at least three times per genotype. P<0.001 for all curves relative to *daf-2*, by log-rank test. **b,** Neuronal expression of *spr-3* and *spr*-4 mediate lifespan extension in *daf-2* mutant worms. Shown are lifespans of worms with neuronal targeting of RNAi by neuronal expression of a *sid*-1 transgene in otherwise *sid-1* null *daf-2(1370)* mutants, or untargeted RNAi in *sid-1* wild-type *daf-2(1370)* mutants. Lifespan effect of neuronal targeting of *spr-4;3* RNAi versus EV control RNAi is significant by log rank test (P=2.5e-6), n=22-56 worms per curve replicated at least 4 times. **c**, SPR-3 and SPR-4 repress genes that mediate neural excitation. Shown are significantly enriched GO terms for upregulated genes related to neural excitation in RNA-seq analysis of day 2 *spr-4;3;daf-2* triple mutants versus *daf-2* single mutant worms. P-values were calculated using Fisher's exact test (see Methods), n=3 biological replicates per genotype.

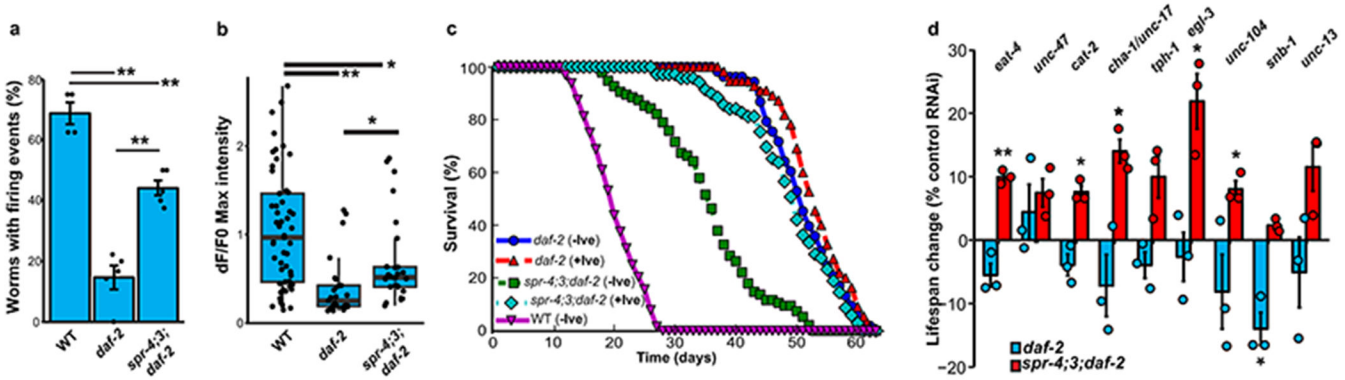

Figure 4.

SPR-3 and SPR-4 suppress multiple neurotransmitter and neuropeptide systems to extend lifespan in *daf-2* mutant worms. **a,** Neural excitation is suppressed in *daf-2* mutants and partially restored by *spr-4;3* mutations. GCaMP imaging was performed in ASH neurons. Shown is the fraction of worms with at least 1 firing event in a 2 minute recording. Values represent the mean ± S.E.M., n= 4-5 independent experiments. **P=7.9e-07 (*daf-2* vs WT), P=1.5e-4 (*spr-4;3;daf-2* vs *daf-2*); P= 0.0011(*spr-4;3;daf-2* vs WT) by ANOVA with post-hoc Tukey test. **b,** Quantification of GCaMP fluorescence changes in day 2 worms: WT, n=53; *daf-2*, n=25; *spr-4;3;daf-2*, n=26. **P=3.1e-6 (*daf-2* vs WT), P=1.5e-3 (*spr-4;3;daf-2* vs *daf-2*); *P=0.018 (*spr-4;3;daf-2 vs* WT) , Mann–Whitney U test with multiple testing correction by Holm's method. **c**, Inhibition of neural excitation by ivermectin (+Ive, 10 pg/ml) reverses lifespan reduction by *spr-4;3* mutations in *daf-2* mutant worms (P=1.1e-16 *spr-4;3;daf-2* +Ive versus -Ive) *daf-2*-Ive, n=53 worms; *daf-2*+Ive, n=55; *spr-4;3;daf-2*-Ive, n=95; *spr-4;3;daf-2*+Ive, n=69; *WT-Ive*, n=64. **d,** Multiple neurotransmitter and neuropeptide signaling systems contribute to the effects of *spr-4;3* mutants on longevity. Change in lifespan of *spr-4;3;daf-2* triple mutant and *daf*-2 single mutant worms following neuronal RNAi for the indicated genes relative to empty vector control RNA. RNAi was targeted to neurons as described in Fig. 3b. *P<0.05, **P<0.01, Student's *t*-test. n=3 independent experiments per group. Individual statistics are in Supplementary Table 22.

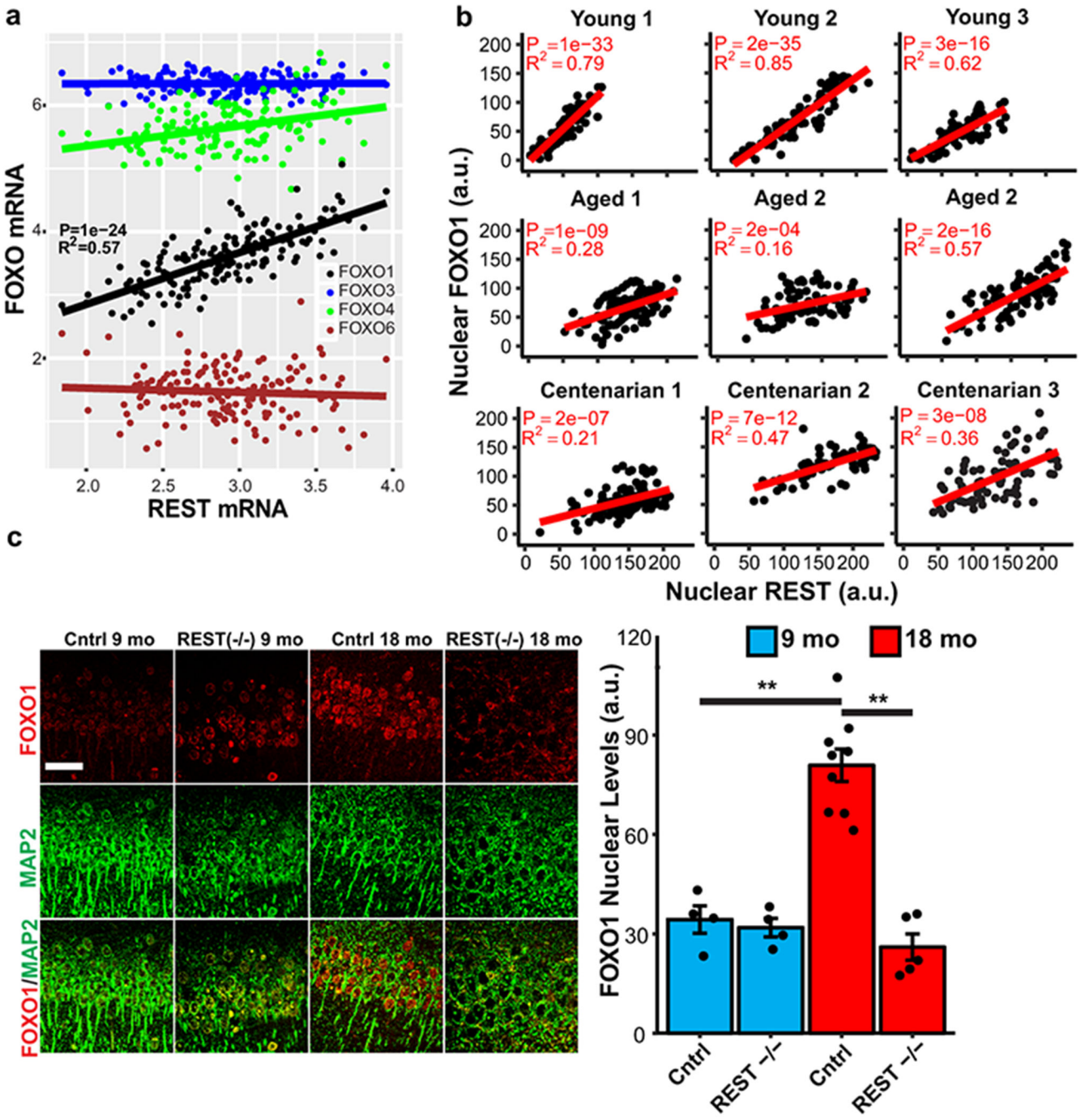

Figure 5.

REST regulates FOXO1 expression in the mammalian brain. **a,** Linear regression analysis of REST and FOXO1 mRNA expression in the prefrontal cortex of cognitively intact individuals (ROSMAP cohort age 71-101 years, n=150) determined by RNA sequencing. P-values were derived by linear regression t-tests for the slope with Bonferroni correction for all expressed genes. **b,** Coordinate regulation of REST and FOXO1 in human prefrontal cortex. Nuclear REST and FOXO1 protein levels were determined by immunofluorescence microscopy in pyramidal neurons of the prefrontal cortex in individual young adult (20-38

yrs), aged (70-80 yrs), and centenarian (>100 yrs) cases. Each point represents a neuron double-labeled for REST and FOXO1. n=71-114 neurons per individual, P-values were derived as in **a**. **c,** FOXO1 induction in the aging mouse cortex is REST-dependent. Left panel: Immunocytochemical labeling for FOXO1 and the neuronal marker MAP2 in cortical neurons of $REST^{lx/lx}$ (Control) and Nestin-Cre;$REST^{lx/lx}$ (REST−/−) mice at 9 and 18 months of age. Scale bar is 40 μm. Right panel: Quantitation of FOXO1 nuclear levels. Values represent the mean ± S.E.M. Control 9 mo: n = 4 mice; Control 18 mo: n = 9 mice; $REST^{-/-}$ 9 mo: n = 4 mice; $REST^{-/-}$ 18 mo: n = 5 mice. **P=1.2e-5 cntrl 9 mo vs cntrl 18mo; **P=4.4e-7 cntrl 18 mo vs REST−/− 18 mo by ANOVA with post-hoc Tukey test.